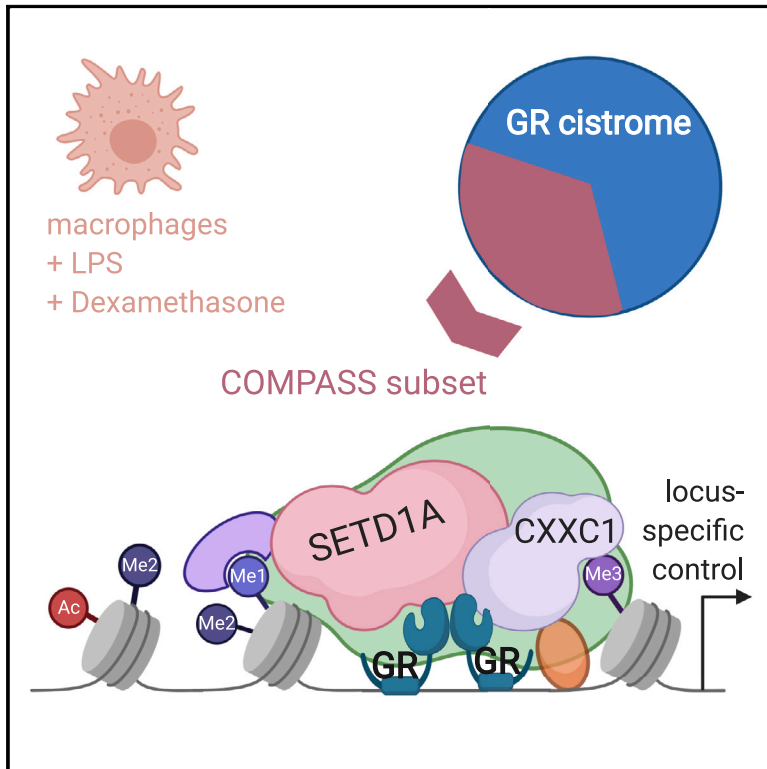# The glucocorticoid receptor recruits the COMPASS complex to regulate inflammatory transcription at macrophage enhancers

Graphical Abstract

Authors

Franziska Greulich, Michael Wierer, Aikaterini Mechtidou, Omar Gonzalez-Garcia, N. Henriette Uhlenhaut

Correspondence

henriette.uhlenhaut@tum.de

In Brief

Glucocorticoids such as dexamethasone are widely used immunomodulators. Combining proteomics, ChIP-seq, RNA-seq, and genetic loss-of-function studies in murine macrophages, Greulich et al. show that recruitment of the SETD1A/COMPASS complex to *cis*-regulatory elements by the glucocorticoid receptor mediates some of their anti-inflammatory actions.

Highlights

- GR's transcriptional complex in macrophages includes COMPASS proteins

- GR ligand changes SETD1A chromatin occupancy in activated macrophages

- Subsets of GR target sites show COMPASS binding and H3K4 methylation dynamics

- SETD1A is required for some of GR's anti-inflammatory actions

CellPress

Cell Reports

Resource

The glucocorticoid receptor recruits the COMPASS complex to regulate inflammatory transcription at macrophage enhancers

Franziska Greulich,[1,2] Michael Wierer,[3] Aikaterini Mechtidou,[1] Omar Gonzalez-Garcia,[1]
and N. Henriette Uhlenhaut[1,2,4,5,6,*]
[1]Institute for Diabetes and Obesity (IDO) & Institute for Diabetes and Cancer (IDC), Helmholtz Center Munich (HMGU) and German Center for Diabetes Research (DZD), 85764 Neuherberg (Munich), Germany
[2]Metabolic Programming, School of Life Sciences Weihenstephan, ZIEL - Institute for Food & Health, Technische Universitaet Muenchen (TUM), 85354 Freising, Germany
[3]Department of Proteomics and Signal Transduction, Max Planck Institute of Biochemistry, 82152 Martinsried, Germany
[4]Metabolic Biochemistry and Genetics, Gene Center, Ludwig-Maximilians-Universitaet LMU, 81377 Munich, Germany
[5]Twitter: @uhlenhautlab
[6]Lead contact
*Correspondence: henriette.uhlenhaut@tum.de
https://doi.org/10.1016/j.celrep.2021.108742

SUMMARY

Glucocorticoids (GCs) are effective anti-inflammatory drugs; yet, their mechanisms of action are poorly understood. GCs bind to the glucocorticoid receptor (GR), a ligand-gated transcription factor controlling gene expression in numerous cell types. Here, we characterize GR's protein interactome and find the SETD1A (SET domain containing 1A)/COMPASS (complex of proteins associated with Set1) histone H3 lysine 4 (H3K4) methyltransferase complex highly enriched in activated mouse macrophages. We show that SETD1A/COMPASS is recruited by GR to specific *cis*-regulatory elements, coinciding with H3K4 methylation dynamics at subsets of sites, upon treatment with lipopolysaccharide (LPS) and GCs. By chromatin immunoprecipitation sequencing (ChIP-seq) and RNA-seq, we identify subsets of GR target loci that display SETD1A occupancy, H3K4 mono-, di-, or tri-methylation patterns, and transcriptional changes. However, our data on methylation status and COMPASS recruitment suggest that SETD1A has additional transcriptional functions. *Setd1a* loss-of-function studies reveal that SETD1A/COMPASS is required for GR-controlled transcription of subsets of macrophage target genes. We demonstrate that the SETD1A/COMPASS complex cooperates with GR to mediate anti-inflammatory effects.

INTRODUCTION

Inflammation is a cellular response to injury or infection, characterized by the secretion of cytokines, chemokines, and other signaling molecules to limit infection, attract immune cells to the site of injury, and orchestrate damage repair (Turvey and Broide, 2010). Excessive activation or impaired silencing of these initially beneficial reactions contributes to a variety of severe human disorders, such as sepsis, arthritis, asthma, etc. (Nathan and Ding, 2010). Therefore, understanding the mechanisms controlling inflammation may enable the development of immunomodulatory therapies.

Glucocorticoids (GCs), such as cortisone or dexamethasone (Dex), are widely prescribed anti-inflammatory drugs that activate the nuclear receptor glucocorticoid receptor (GR) (Oakley and Cidlowski, 2013). Ligand-bound GR translocates to the nucleus to control target gene expression through GC response elements (GREs) or other binding sites present in promoters or enhancers. GR recruits transcriptional coregulators and

enzymes, such as histone acetyltransferases (HATs) or histone deacetylases (HDACs), chromatin remodelers, p160 proteins, histone lysine methyltransferases (KMTs), and demethylases (KDMs), etc., to regulate transcription either positively or negatively (Ito et al., 2000; Chen and Roeder, 2007; Chinenov et al., 2008; Uhlenhaut et al., 2013; Hua et al., 2016; Sacta et al., 2018; Clark et al., 2019). In fact, the details of how GR functions are inherently complex, and its presence in many cells and tissues makes selective pharmacological targeting difficult.

GR binds to distinct *cis*-regulatory elements in a tissue-specific manner (Gross and Cidlowski, 2008). These cistromes arise from the pre-defined accessibility of certain chromatin loci, established by lineage-specific pioneer transcription factors (John et al., 2011; Grøntved et al., 2013; Greulich et al., 2016). Within the same cell type, GR may also regulate target genes in a locus- or signal-specific manner (Rollins et al., 2017; Sacta et al., 2018; Hemmer et al., 2019). GR uses discrete molecular mechanisms and varying coregulators in conjunction with local chromatin contexts for gene-specific transcriptional control (Sacta et al., 2018).

To identify the components mediating GR's immunomodulatory functions, we performed interactome mapping by proteomics, identifying the COMPASS (complex of proteins associated with Set1) complex as a major GR interactor. This conserved protein family catalyzes different stages of histone H3 lysine 4 methylation (H3K4me), a histone mark associated with gene and enhancer activation (Briggs et al., 2001; Nagy et al., 2002). COMPASS complexes are generally composed of multiple subunits including WDR5, ASH2L, DPY30, and RBBP5 (Shilatifard, 2012; Couture and Skiniotis, 2013). Subunits specific to the SETD1A (SET domain containing 1A)/COMPASS complex are WDR82 and CXXC1 (Lee and Skalnik, 2005, 2008; Wu et al., 2008). SETD1A/COMPASS has been associated with global H3K4me3, mostly, but not exclusively, of promoter regions (Wu et al., 2008; Clouaire et al., 2012; Bledau et al., 2014).

In general, H3K4me3 is deposited at the transcriptional start site (TSS) of highly expressed genes (Santos-Rosa et al., 2002; Shilatifard, 2012). Tri-methylation of H3K4 requires a H3K4me2 substrate, which is also established by SETD1A, and expands downstream into the gene body (Soares et al., 2017; Yang and Ernst, 2017). However, a causal relationship between H3K4me3 and transcription has not been definitely established. H3K4me3 has also been proposed to recruit chromatin remodelers, HAT and HDAC complexes, histone demethylases, and the transcription factor II D (TFIID) complex (Briggs et al., 2001; Li et al., 2006; Wysocka et al., 2006; Sims et al., 2007; Vermeulen et al., 2007; Bian et al., 2011; Beurton et al., 2019).

H3K4me1 and H3K4me2 mainly mark enhancers that are MLL3/4 dependent, occasionally with low levels of H3K4me3 (Vermeulen et al., 2007; Pekowska et al., 2011; Kaikkonen et al., 2013). A function for SETD1A/COMPASS in enhancer methylation has not been shown, but studies in yeast, in *Drosophila*, and in mice demonstrate its crucial role in global H3K4me (Ardehali et al., 2011; Bledau et al., 2014; Soares et al., 2014). However, yeast SET1 is dispensable for cellular survival under steady-state conditions (Briggs et al., 2001; Boa et al., 2003).

Here, we identified the SETD1A/COMPASS complex as a coregulator in GR-mediated inflammatory gene regulation. We observed that GR recruits the SETD1A/COMPASS complex to control a subset of enhancers in activated macrophages. SETD1A/COMPASS recruitment to chromatin coincided with binding-site specific changes, but not with global changes, in H3K4me. *Setd1a* depletion in macrophages confirmed its requirement for locus-dependent, GR-mediated gene regulation, without loss of H3K4me status. We therefore suggest that SETD1A contributes to GR's anti-inflammatory actions, independently of H3K4me, in a gene-specific manner.

RESULTS

SETD1A/COMPASS interacts with the GR in macrophages

In order to identify the GR nuclear interactome under inflammatory conditions, we performed chromatin immunoprecipitation coupled to mass spectrometry (ChIP-MS) in primary murine bone-marrow-derived macrophages (BMDMs). Cells were treated with the GR ligand Dex and the Toll-like receptor 4

(TLR4) stimulus lipopolysaccharide (LPS), which activates nuclear AP-1, nuclear factor κB (NF-κB), and interferon (IFN) regulatory factors (IRFs). Significantly enriched proteins are shown in Figure 1A ($p < 0.05$, >1.5-fold enrichment over immunoglobulin G [IgG] controls; Table S1).

We confirmed known interactions with NCOA2/GRIP1, CBP/P300, and the NF-κB subunits c-Rel (REL) and p65 (RELA) (Ray and Prefontaine, 1994; Kino et al., 1999; Wang et al., 2012; Uhlenhaut et al., 2013; Rollins et al., 2017). We detected all the components of the SETD1A/COMPASS complex, namely SETD1A, SETD1B, WDR5, ASH2L1, RBBP5, DPY30, CXXC1, and WDR82, among GR's direct or indirect physical partners in the presence of LPS + Dex (Figure 1A). Gene Ontology (GO) analysis revealed H3K4me among the main functionalities of the GR interacting proteins (Figure 1B).

These data were confirmed by co-immunoprecipitation (coIP) in the macrophage cell line RAW264.7 (Figure 1C; Figures S1A and S1B). coIP with a GR-specific antibody co-enriched the catalytic subunit SETD1A, CXXC1, and WDR82. Using a SETD1A-specific antibody, we validated the interaction of SETD1A, CXXC1, and WDR82 with GR. Conversely, CXXC1 and WDR82 coIPs also enriched GR (Figure 1C).

We also found SETD1A, CXXC1, and COMPASS subunits co-enriched in our ChIP-MS interactome from mouse livers, suggesting that these interactions occur *in vivo* and are not only macrophage specific (Figure S1C) (Hemmer et al., 2019).

To characterize the functional relationships between SETD1A, SETD1B, and GR, we generated conditional *Setd1b* knockouts (Bledau et al., 2014). (We could not obtain viable *Setd1a* null macrophages, suggesting that *Setd1a* is essential for cell survival.) *Setd1b* knockout macrophages were differentiated, treated with either LPS or Dex + LPS, and processed for RNA-seq (Figure S1D). We did not detect major differences in GR target gene regulation between wild-type and *Setd1b* knockout macrophages in response to GR ligand (Figure S1E). Thus, SETD1B may not be critical for GC-induced transcriptional responses. We therefore focused on SETD1A for further functional analyses.

GR and SETD1A/COMPASS co-occupy genomic regions in macrophages

To understand the function of the protein-protein interactions between GR and SETD1A/COMPASS in macrophages under inflammatory conditions, we tested whether SETD1A, CXXC1, and GR co-occupy genomic loci in murine BMDMs using ChIP-seq. In macrophages treated with LPS + Dex, 42% of the GR binding sites (GBSs) were co-occupied by SETD1A, of which 60% additionally bound CXXC1 (Figure 2A).

Bioinformatic motif analyses confirmed the central enrichment of various GRE motifs in all genomic regions bound by GR. In addition to palindromic GREs (NGNACA(N)$_3$TGTNCN) with three spacer nucleotides (Strähle et al., 1987), the subset of regions binding GR, SETD1A, and CXXC1 was enriched for GRE sequences with only one spacer nucleotide (GNNACA(N)$_1$TGTNNC, log(p value) of $2.7e^{-4}$) (Figure 2B). These results suggest that co-recruitment of CXXC1 with SETD1A by GR may involve specific GRE sequences.
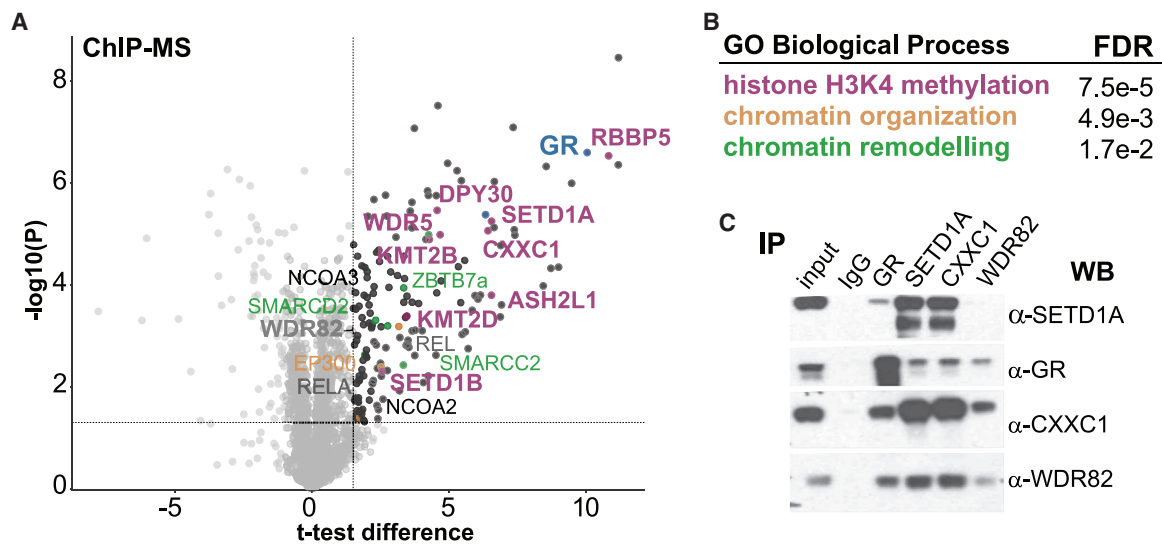
Figure 1. SETD1A/COMPASS interacts with the glucocorticoid receptor (GR)
(A) ChIP-MS proteomics. Volcano plot shows proteins enriched in the GR coIP. Each dot is a detected protein. Dashed lines and darker colors delineate the threshold of 1.5-fold enrichment and p < 0.05 significance (n = 3). Selected proteins belonging to over-represented Gene Ontology (GO) categories (B) are labeled in color.
(B) GO functional annotation of significantly co-enriched proteins (p < 0.05, fold change [FC] > 1.5).
(C) Western blots of endogenous coIPs for GR, SETD1A, CXXC1, and WDR82 in RAW264.7 cells treated with Dex + LPS.

Genomic regions bound by SETD1A without co-occupancy of CXXC1 or GR were enriched for ETS motifs, and SETD1A-CXXC1 co-occupied regions were enriched for YY1 motifs (Figure 2B). Both ETS and YY1 motifs are usually associated with promoters, consistent with these SETD1A-binding regions mapping close to TSSs (Figure 2C). Most GR-bound subsets, including those without co-binding COMPASS proteins, mapped to intergenic locations (Figure 2C), agreeing with previous results showing GR mainly binds distant enhancers in macrophages (Uhlenhaut et al., 2013).

Other motifs co-enriched among all GR-occupied sites, within 100 bp of the peak center, included the pioneer factor PU.1 (Figure S2E), a lineage-determining pioneer factor known to shape the myeloid chromatin landscape (Heinz et al., 2010). Furthermore, regions co-bound by GR-SETD1A-CXXC1 also featured AP-1 motifs, a known interaction partner of GR (Jonat et al., 1990; Yang-Yen et al., 1990). By contrast, GR-SETD1A co-bound sites were enriched for C/EBP and RBPJ motifs, suggesting there may be different modes of transcription factor crosstalk for distinct subsets of enhancers. In the absence of GR, SETD1A- or SETD1A-CXXC1-bound sequences mostly localized to promoters and thus were enriched for SP1 motifs, as was shown for CG-rich promoter elements (Dynan and Tjian, 1983). Common SETD1A-CXXC1-bound sites found in macrophages treated only with LPS contained NF-κB and AP-1 motifs and mapped to inflammatory signaling pathways, indicating that the COMPASS complex might be involved in the LPS response itself (Figures S2A–S2D).

Having identified different groups of genomic loci involved in the combinatorial recruitment of GR, SETD1A, and CXXC1 in BMDMs under Dex + LPS conditions, we assigned biological functions to these regions by KEGG (Kyoto Encyclopedia of Genes and Genomes) pathway over-representation analysis. All the sites co-occupied by GR-SETD1A-CXXC1 were associated with inflammatory pathways (Figure 2D), consistent with GR's immunomodulatory activity (Uhlenhaut et al., 2013; Escoter-Torres et al., 2019). Sites bound by GR alone were associated with Ca²⁺ signaling, endocytosis, and cell cycle, and sites bound by SETD1A alone were enriched for protein degradation and processing pathways (Figure 2D). Thus, SETD1A/COMPASS proteins are associated with the anti-inflammatory properties of GCs.

Altogether, GR, SETD1A, and, to a lesser extent, CXXC1 co-occupy genomic loci in macrophages treated with Dex + LPS. These common *cis*-regulatory regions were mostly intergenic, demonstrating that the SETD1A/COMPASS complex is bound to mammalian enhancers *in vivo* (van de Lagemaat et al., 2018; Mukai et al., 2019). However, this co-occupancy only represents a fraction of the GR cistrome, indicating that diverse functional classes or categories of regulatory sites likely exist.

GR recruits SETD1A/COMPASS to chromatin in response to ligand

To determine whether genomic SETD1A/COMPASS binding was influenced by GC treatment, we compared the SETD1A and CXXC1 ChIP-seq signals in macrophages treated either with LPS alone or with Dex + LPS. (As we were most interested in the regulation of inflammatory genes by GR, we did not investigate quiescent macrophages without LPS stimulation [vehicle or Dex only].) We found that the addition of GR ligand substantially increased the genomic occupancy of both SETD1A and CXXC1, in a manner similar to known GR coregulators, such
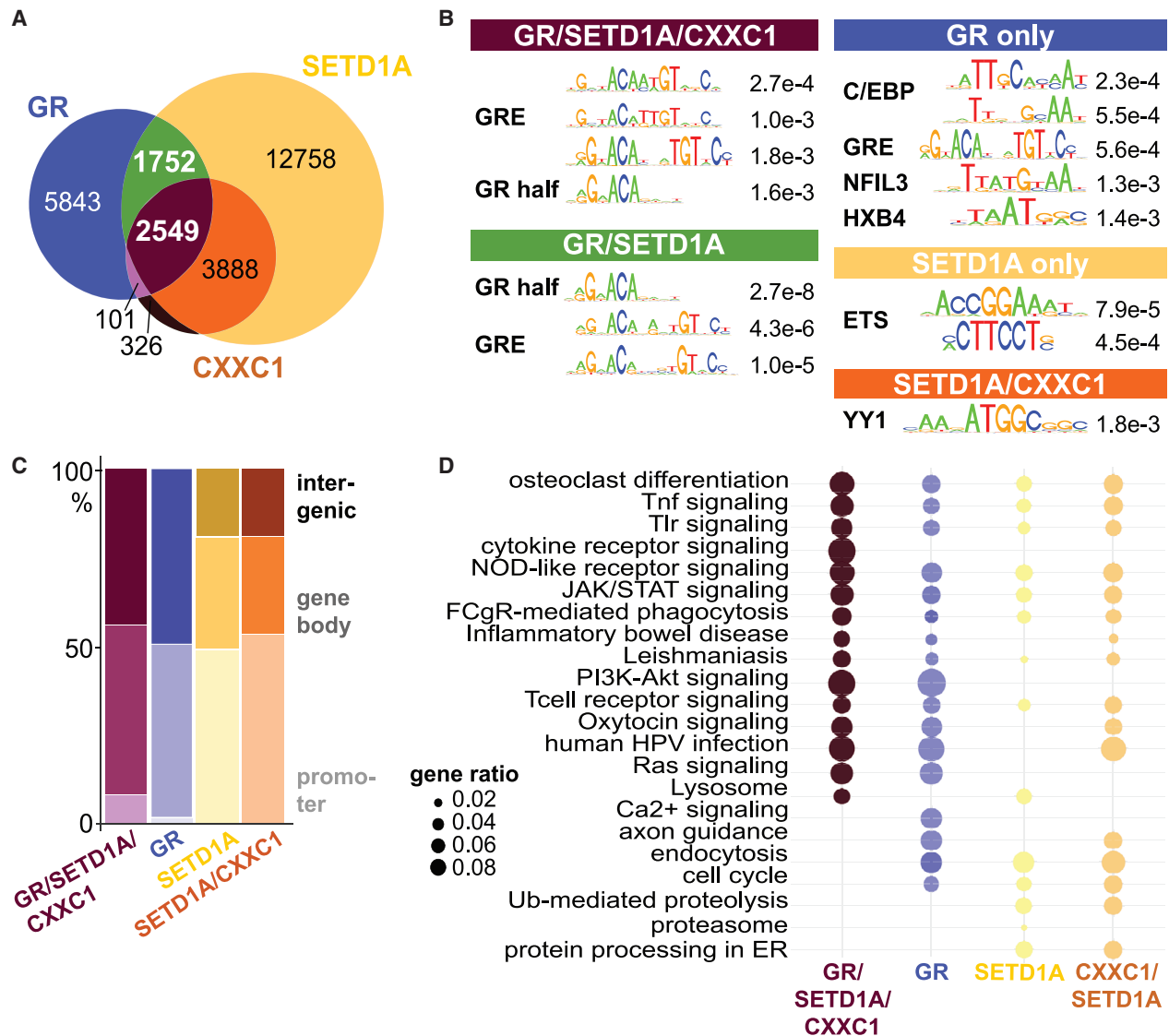
Figure 2. GR and SETD1A/COMPASS co-occupy genomic regions in macrophages
(A) Venn diagram of GR (blue, n = 3), SETD1A (yellow, n = 2), and CXXC1 (brown, n = 2) ChIP-seq peak overlap in macrophages treated with Dex + LPS.
(B) Differential Centrimo motif enrichment of indicated subsets over the total called 27,127 GR, SETD1A, and CXXC1 peaks, with Bonferroni-adjusted (adj) binomial p values (right).
(C) Feature distribution over genomic locations of the different peak subsets (promoters defined as <1 kb from the TSS, intergenic defined as >1 kb from any gene).
(D) KEGG pathway over-representation analysis for peak subsets (Benjamini-Hochberg adj hypergeometrical p value). Circle sizes represent gene ratios.

as NCOA2/GRIP1 (Figure 3A; Figures S3A and S3B) (Uhlenhaut et al., 2013). We then analyzed 1,765 intergenic regions (>1 kb from any gene) bound by both GR and SETD1A in response to Dex, as revealed by ChIP-seq. We plotted the SETD1A and CXXC1 occupancy at the GR target sites in descending order of GR-dependent SETD1A recruitment. Numerous sites gained SETD1A centrally at the GBS, while most other signals appeared peripherally near the GBS (Figure 3A). Similar results were obtained for CXXC1, suggesting that SETD1A and CXXC1 are recruited to chromatin by GR in response to ligand (Figure 3A).

GC-induced SETD1A/CXXC1 recruitment was seen at the anti-inflammatory GR target genes *Tsc22d3* (*Gilz*) and *Dusp1* (Figure 3B; Figure S3C). Cytokines or chemokines, such as the GR targets *Cxcl10* or *Il1a*, which are suppressed by GCs, however, did not show altered SETD1A or CXXC1 occupancy at their GR-bound enhancers after Dex stimulation. The binding of SETD1A and CXXC1 over the gene body of *Cxcl10* was reduced by Dex (Figure 3B; Figure S3C), in line with previous characterizations of SETD1A promoter binding and with known correlations between active transcription and H3K4me3 levels (Nagy et al., 2002; Santos-Rosa et al., 2002; Sims et al., 2007; Shilatifard 2012).
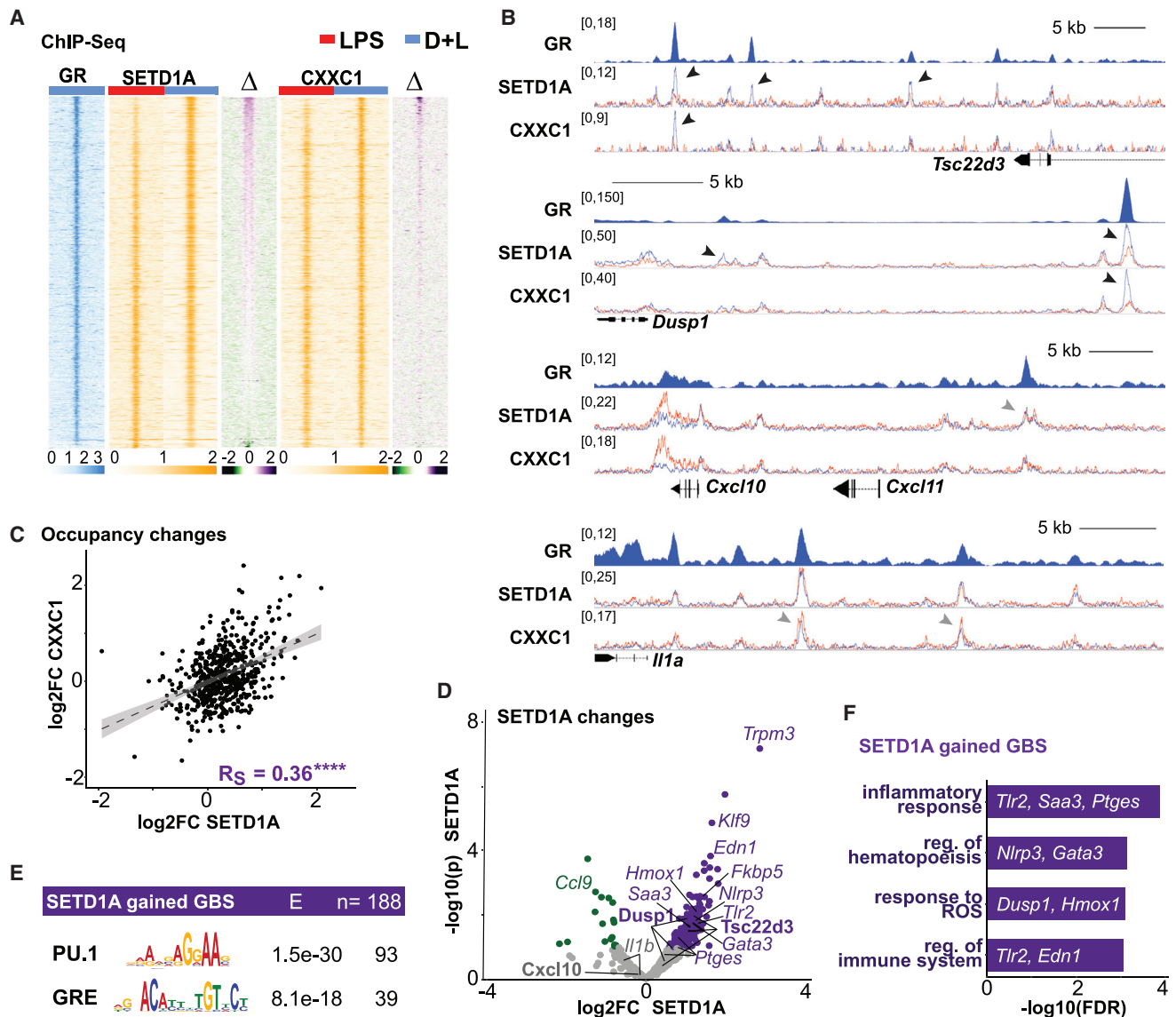
Figure 3. GR recruits SETD1A/COMPASS to chromatin in response to ligand

(A) Heatmap of mean GR, SETD1A, and CXXC1 ChIP-seq coverage in Dex + LPS- and LPS-treated macrophages (n = 2). Each line is one GR-bound site ±2 kb. Binding sites are sorted by log2FC of SETD1A occupancy between Dex + LPS and LPS. Δ represents the difference in normalized coverage between Dex + LPS and LPS.

(B) Example genome browser tracks of ChIP-seq for GR, SETD1A, and CXXC1 in macrophages treated with LPS or Dex + LPS. GR occupancy is the filled area under the curve (blue) (n = 1). Lines are medians of two replicates. Arrows point toward signal changes.

(C) Correlation of SETD1A and CXXC1 occupancy at GR-SETD1A-CXXC1 co-bound enhancers; scatterplot of log2FC of CXXC1 and SETD1A. The dashed regression line includes the 95% confidence interval (gray shadow). ****$p < 0.0001$. R_S, Spearman correlation coefficient.

(D) Changes in SETD1A occupancy (log2FC$_{SETD1A}$) in response to Dex + LPS over LPS. GBSs with increased SETD1A occupancy (FC > 1.5, p < 0.1) are purple; GBSs with reduced SETD1A binding (FC < −1.5) are green. Selected enhancers are labeled.

(E) MEME motif enrichment of sites recruiting SETD1A (p < 0.1, FC > 1.5), with E-values and numbers of positive sites.

(F) GO analysis for biological processes of the closest genes, with examples and the −log10 of the hypergeometric false discovery rate (FDR).

Overall, the changes in SETD1A and CXXC1 recruitment to intergenic regions co-bound by GR-SETD1A-CXXC1 correlated well for the recruitment of both factors (Spearman correlation coefficient of 0.36) (Figure 3C). We classified the GR-SETD1A sites into those significantly gaining SETD1A (>1.5-fold, p < 0.1), those with unchanged occupancy (p < 0.1, fold change [FC] < 1.5×),

and those losing SETD1A (p < 0.1, FC < −1.5×). CXXC1 occupancy was similar to SETD1A, with enhancers gaining SETD1A also gaining CXXC1 and enhancers losing SETD1A also losing CXXC1 binding (Figure S3D). This co-dependency of SETD1A and CXXC1 recruitment is consistent with their known function within the same complex and with the observation that CXXC1

is required for SETD1A recruitment at promoters (Brown et al., 2017; van de Lagemaat et al., 2018).

Analysis of SETD1A enrichment at GR enhancers by differential binding analysis revealed that those loci gaining SETD1A correspond to GR target genes, such as *Tsc22d3*, *Dusp1*, *Fkbp5*, and *Klf9* (Figure 3D). These are known GR-dependent genes in macrophages and are enriched for the palindromic GRE and PU.1 motifs (Figure 3E) (Uhlenhaut et al., 2013; Rollins et al., 2017; Escoter-Torres et al., 2019). These enhancers were significantly enriched for the biological processes "inflammatory response" (*Tlr2*, *Ptges*), "response to reactive oxygen species" (*Dusp1*, *Hmox1*), "positive regulation of the immune system" (*Nlrp3*), and "regulation of hematopoiesis" (*Gata3*) (Figure 3E; Table S3). The small number of sites that lost SETD1A upon GR binding did not show any enrichment for specific motifs or GO terms.

Since we had also detected COMPASS components in our liver ChIP-MS interactome, we tested whether the occupancy of SETD1A and CXXC1 was dependent on GR *in vivo*. Indeed, we found reduced binding of both SETD1A and CXXC1 to GR target sites in livers from hepatocyte-specific GR knockout mice (Figure S3E).

In sum, we found that ligand-induced GR chromatin occupancy leads to the recruitment of the SETD1A/COMPASS H3K4 methyltransferase complex to a subset of GR-bound *cis*-regulatory elements. These GC-activated enhancers control inflammatory responses and represent a distinct subset of the GR cistrome.

GR-mediated SETD1A/COMPASS recruitment to enhancers shows locus-specific histone methylation

To assess whether ligand-dependent recruitment of SETD1A/COMPASS to GR target sites changed mono-, di-, and tri-methylation patterns in activated cells, we used ChIP-seq in primary macrophages treated either with LPS or with Dex + LPS. H3K27ac was measured as a modification associated with active enhancers, and RNA-seq was used to determine target gene transcription (Creyghton et al., 2010). We performed model-based clustering of log2 FCs in SETD1A, CXXC1, H3K4me1/me2/me3, and H3K27ac ChIP-seq signals for GBSs with significantly altered SETD1A binding (absolute [abs](FC) > 1.5, p < 0.1) in Dex + LPS- versus LPS-treated BMDMs. We assumed heterogeneity among the GR enhancers with differential SETD1A binding and therefore chose generalized mixed models. The appropriate model was selected by maximizing the Bayesian information criterion (Scrucca et al., 2016). A model with three components and ellipsoidal distribution with variable volume and equal shape fitted the data best and was used to classify target sites (Figure S4A).

This analysis revealed three clusters of epigenetic changes, correlating with the recruitment of SETD1A to GR enhancers. Two clusters gained SETD1A occupancy, and the smallest cluster lost SETD1A upon Dex + LPS treatment (Figures 4A–4D). Consistent with our previous results, GR enhancers significantly gaining SETD1A (p < 0.0001) also acquired CXXC1 and H3K27ac and were associated with nearby genes that mainly increased mRNA expression upon Dex stimulation (Figures 4B and 4E). Note that one cluster (22 loci, red) additionally gained H3K4me2

in response to ligand (Figure 4B, Figure S4C). These loci represent the fraction of sites that recruited SETD1A *de novo*, such as *Tsc22d3* (Figures 3B, 4C, and 4D; Figures S4B and S4C). Those enhancers with reduced SETD1A binding upon Dex treatment lost CXXC1, H3K4me3, and H3K27ac (21 sites, blue) (Figures 4A and 4B). Similar results were obtained by model-based clustering and correlation analysis of these differential target sites, with increased gene expression corresponding to gaining SETD1A and H3K27ac, independent of H3K4me2 or H3K4me3 (Figures 4E and 4F; Figures S4C and S4D).

These data highlight the existence of locus- and factor-specific modes of regulation. For instance, the *Tsc22d3* enhancer showed increased H3K4me1/me2/me3 and H3K27ac, while the *Dusp1* enhancer showed almost no significant changes in H3K4me (with the exception of H3K4me3) or H3K27ac. The *Cxcl10/11* and *Il1a* enhancers, with constant SETD1A occupancy unaffected by ligand, only showed reductions in H3K27ac and H3K4 mono-methylation, and no changes in di- or tri-methylation (Figure 4C; Figure S4B). The ChIP-seq results were confirmed by spike-in ChIP-qPCR for selected sites. The changes in H3K4me1 at the *Tsc22d3* enhancer were less prominent in ChIP-qPCR, which was normalized to total H3, suggesting that they might result from nucleosome repositioning rather than increased mono-methylation at this particular site (Figure 4D).

H3K4me dynamics upon SETD1A depletion

Investigation of the function of the mammalian SETD1A/COMPASS complex has been complicated by the early lethality of *Setd1a* knockout mice (Bledau et al., 2014). Hematopoietic-cell-specific deletion of *Setd1a* causes loss of hematopoietic differentiation, indicating a requirement of *Setd1a* for cellular identity and development (Tusi et al., 2015). However, its function in fully differentiated cells in response to signaling stimuli has not been explored. To elucidate the functional impact of SETD1A on gene regulation by GR, we generated a *Setd1a* hypomorph using CRISPR-Cas9 in RAW264.7 cells. We truncated SETD1A by introducing a premature stop codon before the essential SET domain, which lowers COMPASS family protein stability (Soares et al., 2014; Dorighi et al., 2017; Jang et al., 2017). Western blots confirmed the reduced SETD1A protein expression in *Setd1a*[Del/+] (*Del*) heterozygous clones (Figures S5A and S5B). We were unable to generate homozygous *Setd1a* deletion mutants, presumably because *Setd1a* null macrophages are not viable, as seen with the floxed BMDMs. The suitability of RAW264.7 cells was confirmed by comparing GR cistromes and target gene expression in primary and RAW264.7 macrophages (Figure S5C). GR binding to the *Tsc22d3* and *Dusp1* enhancers was not affected in *Del* cells (Figure S5D).

To investigate whether *Setd1a* depletion reduced H3K4me1, H3K4me2, or H3K4me3 near common macrophage GR/SETD1A binding sites, we profiled H3K4me1/me2/me3 by ChIP-seq in wild-type and *Del* RAW264.7 cells after either LPS or Dex + LPS stimulation. We excluded global loss of H3K4me1/me2/me3 due to *Setd1a* deletion (Figure S5B) and performed spike-in normalizations for our ChIP-seq samples. The cumulative and median H3K4me1/me2/me3 signals around the GBSs were unaltered by *Setd1a* mutation (Figures 5A and 5C; Figures S5E–S5G).
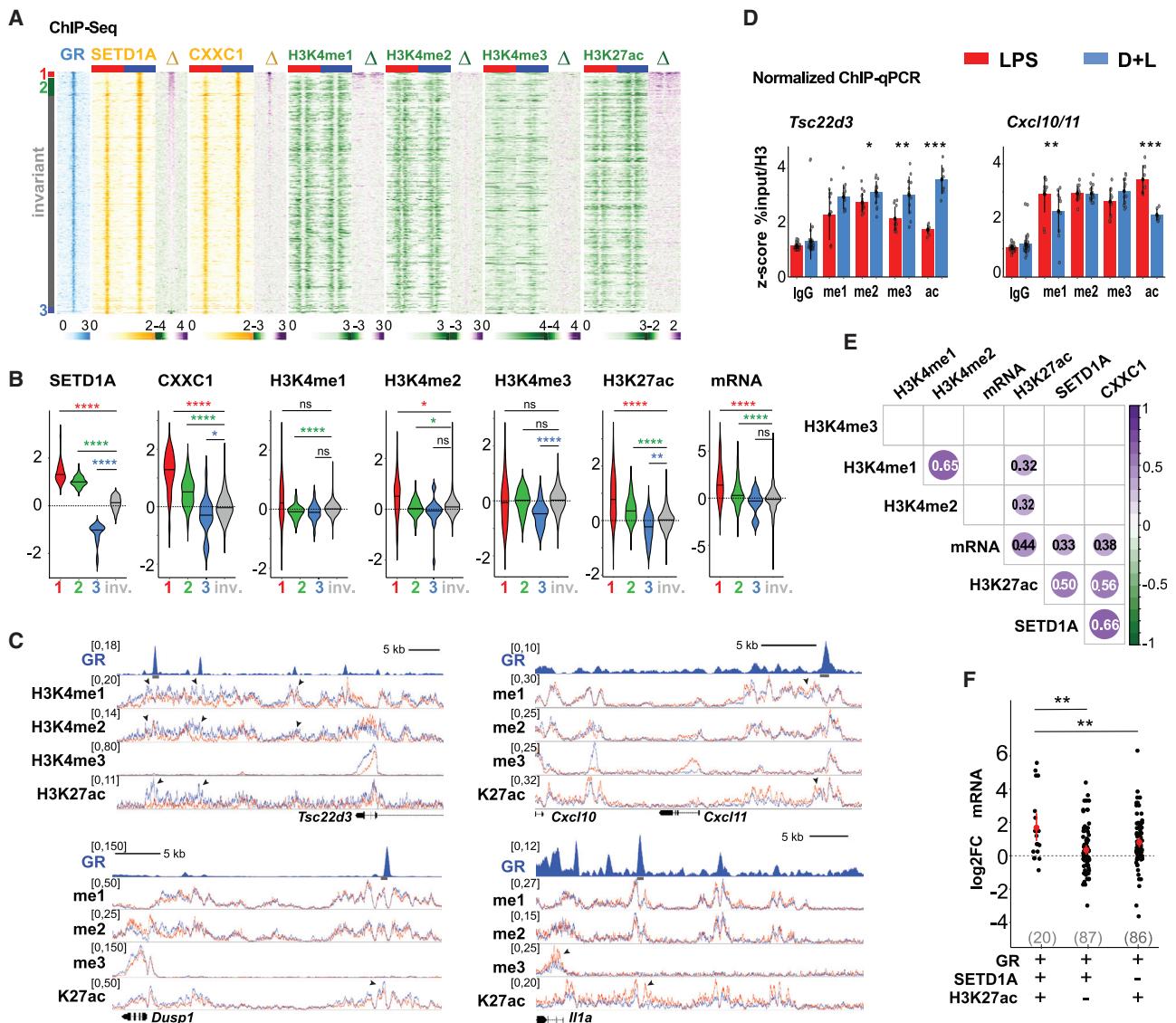
Figure 4. GR-mediated SETD1A/COMPASS recruitment to enhancers shows locus-specific histone methylation

(A) Normalized SETD1A, CXXC1, H3K4me1/me2/me3, and H3K27 acetylation (H3K27ac) ChIP-seq signals in LPS- and Dex + LPS-treated macrophages, ±2 kb around the GBS. Loci are sorted by clusters identified in Figure S4C. Invariant: GBSs with unchanged SETD1A (p > 0.1, −1.5 < FC < 1.5) occupancy, 588 bp around the GBS. Δ represents the coverage difference between Dex + LPS and LPS treatments.

(B) Log2FC in SETD1A, CXXC1, H3K4me1/me2/me3, and H3K27ac ChIP-seq signals at intergenic regions. mRNA expression of the genes closest to the enhancers from cluster 1, cluster 2, and cluster 3 is displayed together with those showing invariant SETD1A occupancy (inv., p > 0.1, −1.5 < FC < 1.5; gray). Black lines indicate the distribution mean. (ChIP-seq: Kruskal-Wallis test with post hoc Dunn's test; RNA-seq: one-way ANOVA with post hoc pairwise two-sided t test, Benjamini-Hochberg adj). n = 2.

(C) Normalized median genome browser tracks for H3K4me1/me2/me3 and H3K27ac ChIP-seq (n ≥ 2, LPS- (red) versus Dex + LPS-treated (blue) BMDMs) plus GR. Arrowheads point at treatment-dependent changes; lines below GR peaks indicate primer locations for (D).

(D) Normalized spike-in ChIP-qPCR for selected loci; mean Z scores of total H3 normalized % inputs. Error bars represent standard deviation (n = 3, two-sided Wilcoxon-Mann-Whitney test).

(E) Correlation plot of log2FC in SETD1A, CXXC1, H3K4me1/me2/me3, and H3K27ac at intergenic GBSs with differential SETD1A occupancy (−1.5 > FC > 1.5, p < 0.1) and the mRNA expression of the closest gene. Pearson correlation coefficients with p < 0.001 are displayed as numbers.

(F) Log2FC in mRNA expression of genes with nearby GBS over changes in SETD1A occupancy and/or H3K27ac levels (+, gain; −, invariant or lost). Each dot reflects one enhancer. Red: mean and 95% confidence intervals (Kruskal-Wallis test with post hoc Dunn's test, Benjamini-Hochberg adj). Enhancer numbers are in parentheses.

A

ChIP-Seq RAW264.7 CRISPR clones

B

C

D
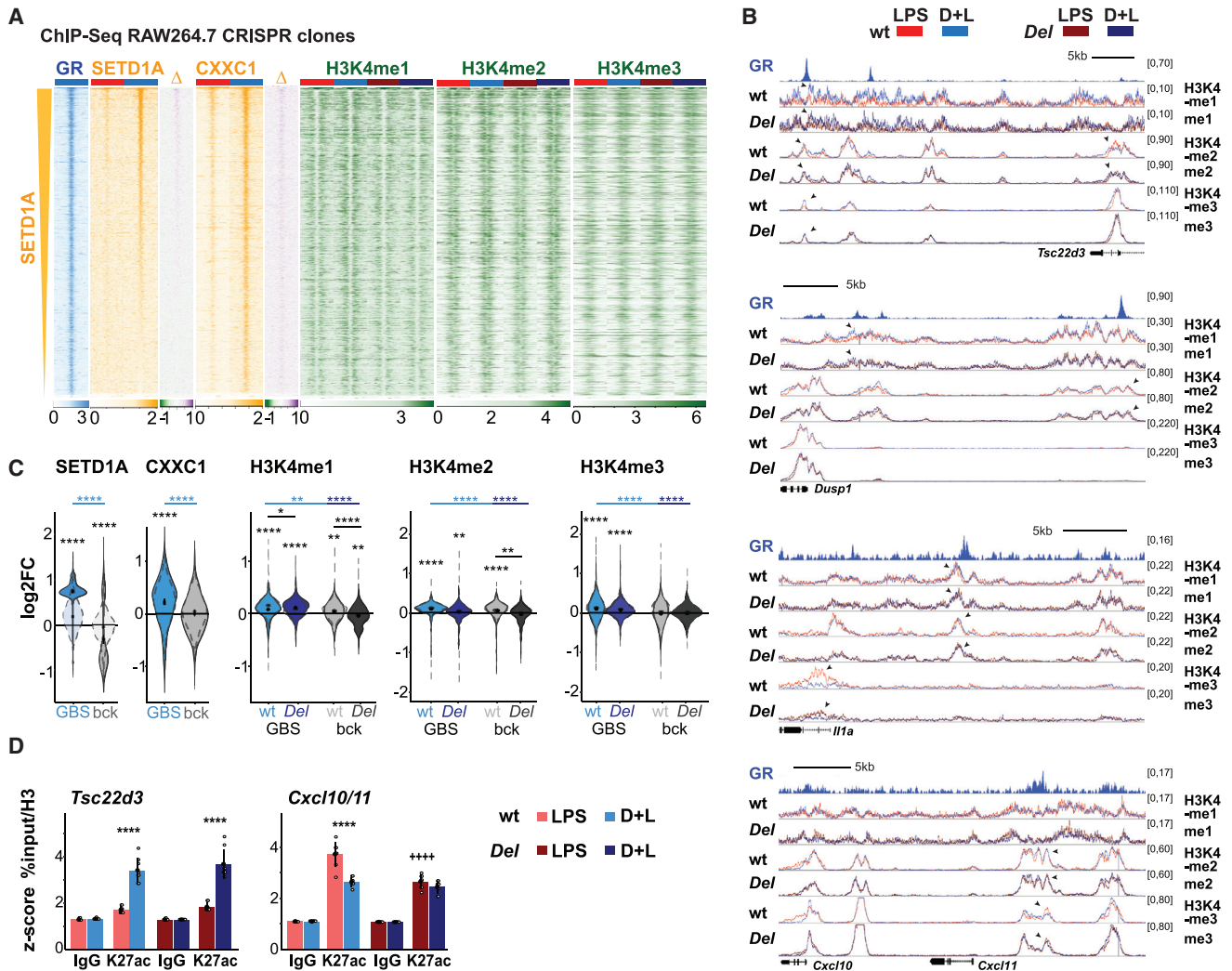
Figure 5. H3K4 methylation dynamics upon SETD1A depletion

(A) Heatmaps for mean SETD1A, CXXC1, and H3K4me1/me2/me3 ChIP-seq at ±2 kb around GR-SETD1A common sites in wild-type (WT) and *Setd1a^{Del/+}* (*Del*) RAW264.7 cells treated with LPS or Dex + LPS. GBSs are sorted by descending SETD1A ChIP signal strength (n = 2–3). See legend (B).

(B) Example genome browser tracks with median ChIP-seq signals for GR, H3K4me1/me2/me3 in WT and mutant RAW264.7 cells. Arrows point towards GR binding sites or changes observed at the TSS.

(C) Violin plots for log2FC in SETD1A, CXXC1, and H3K4me1/me2/me3 ChIP-Seq signals at intergenic regions, comparing Dex + LPS to LPS. GBSs bind GR and SETD1A, while background (bck) sites show H3K4me1/me2/me3, but no GR, SETD1A, or CXXC1 peaks. Signal distributions for constant (light blue, dashed outline) and for GR-SETD1A sites with changed SETD1A binding (full blue, solid outline) are shown (LPS + Dex versus LPS, p < 0.05). Treatment effect was determined by one-sample Wilcoxon-Mann-Whitney test, genotype differences by two-sided Wilcoxon-Mann-Whitney test, and group differences by paired two-sample Wilcoxon-Mann-Whitney test.

(D) Spike-in normalized H3K27ac ChIP qPCR in LPS- or Dex + LPS-treated RAW264.7 cells. Mean Z scores of total H3 normalized % inputs are plotted (n = 3). Error bars represent standard deviations. Kruskal-Wallis with post hoc Dunn's test, with Benjamini-Hochberg adj p values (adj ps). For all graphs, *p < 0.05, **p < 0.01, ***p < 0.001, ****p < 0.0001.

Similar to primary macrophages, H3K4me1/me2/me3 ChIP signals were increased at the *Tsc22d3* enhancer in response to Dex in both wild-type and *Del* cells. We did not observe reductions in H3K4me1/me2/me3 in *Setd1a* mutants at the *Dusp1*, *Tsc22d3*, *Il1a*, or *Cxcl10* loci (Figure 5B; Figures S5H and S5I). H3K27ac was not affected at the *Tsc22d3* or *Cxcl10* enhancers in *Setd1a^{Del/+}* mutants either (Zhang et al., 2020) (Figure 5D).

In summary, we show that GR occupancy, SETD1A recruitment, and increased H3K27ac at a subset of GBSs confer a robust activation potential onto the nearest target gene. However, we did not identify a significant correlation between H3K4me1, H3K4me2, or H3K4m3 and GR-mediated transcriptional control of inflammatory response genes. We conclude that ligand-mediated H3K4me1/me2/me3 dynamics at distant GR-bound sites do not depend on *Setd1a* function. SETD1A depletion did not reduce H3K4 methylation levels, suggesting that the role of SETD1A/COMPASS at enhancers may be distinct from its promoter function and histone methyltransferase activity.

SETD1A mediates regulation of specific myeloid GR targets

To test the hypothesis that SETD1A recruitment by GR plays a role in target gene regulation, we determined the transcriptional effect of *Setd1a* reduction using RNA-seq. The Dex-induced or -repressed mRNA FCs in wild-type and *Setd1a*$^{Del/+}$ RAW264.7 cells stimulated with LPS were compared at two time points (6 and 16 h). We identified 312 ligand-dependent genes that showed an altered Dex response in *Setd1a*$^{Del/+}$ mutants. Four differential response clusters were identified by weighted gene network correlation analysis (Figures 6A and 6B; Figures S6A and S6B).

Cluster 1 contained inflammatory mediators that were repressed by GR in both wild-type and *Del* mutants, albeit with different FCs (Figures 6A–6C). Many of them displayed constant, GC-independent SETD1A occupancy of GBSs in wild-type macrophages, similar to *Cxcl10*, and showed diminished induction by LPS in *Del* mutants. We confirmed the diminished LPS response by qRT-PCR time-series expression analysis of *Cxcl10*, *Irf7*, and *Infb1* in wild-type and *Del* cells (Figure 6D; Figures S6A and S6C). Since *Cxcl10* was expressed at much lower levels in *Del* mutants, it is difficult to interpret GR repression in this case (Figure 6D). However, IFN-β1 treatment rescued the diminished LPS response and induced high levels of *Cxcl10* and *Irf7* expression (Figures S6D–S6F). These observations imply that the genes in cluster 1 may have failed to respond to LPS as a consequence of lost *Infb1* induction in *Del* mutants. Furthermore, when we profiled the mRNA levels of SET domain containing of methyltransferase-encoding genes in LPS and in LPS + IFN-β1-treated control and *Del* cells, we observed differential expression of several enzymes, such as *Setdb2* or *Nsd3*, for example (Figure S6G). These might potentially compensate for SETD1A loss of function and could explain the rescue effect as well.

Similarly, cluster 3 is comprised of inflammatory genes activated by LPS and repressed by Dex and involved in "cytokine production," "response to lipids," "apoptotic signaling," and "response to LPS" (Figure 6C; Table S2). In contrast to cluster 1, the induction of these genes by LPS and their repression by GR were unaltered in *Del* mutants at 6 h, for example, *Tnfa* (Figures 6A and 6B; Figures S6B and S6C).

Clusters 2 and 4 represent genes activated by Dex either early (cluster 2, 6 h) or late (cluster 4, 16 h), among them the anti-inflammatory GR targets *Dusp1* and *Tsc22d3* (Figures 6A–6D). Cluster 4 was enriched for pathways such as "response to bacteria" (Figure 6C; Table S4), and both clusters had a high percentage of genes featuring nearby GR ChIP peaks (Figure S6A). The early induction and the severely diminished or delayed responses of *Dusp1*, *Tsc22d3*, and *Lcn2* to ligand in *Setd1a*$^{Del/+}$ mutants were validated by qRT-PCR at different time points (Figure 6D; Figure S6C). This reduced transcriptional activation was accompanied by a decrease of the Dex-induced H3K4me3 ChIP signals at the TSSs of those targets in *Del* clones (Figures 5B and 6E). However, the genes displaying prominent H3K4me3 signals around their TSSs again only represent a fraction of GR targets. For a global correlation between H3K4me dynamics, transcriptional changes, and SETD1A dependence, we analyzed GR-SETD1A co-bound sites with

detectable H3K4me changes in response to Dex. For these targets, we determined the fraction which either displayed altered H3K4me1/me2/me3 patterns or differential transcript expression of the nearest gene in *Del* mutants (Figure 6E). These results again only show subsets of sites with differential H3K4me and a larger subset of target genes whose transcription is affected by SETD1A depletion.

On the other hand, when studying our defined GR subsets with SETD1A recruitment and H3K4me dynamics (Figure 4B), we found that a significant number of them are associated with nearby genes whose expression was affected by *Setd1a* mutation (Figure 6F).

Taken together, Dex-dependent transcriptional activation was disturbed in *Setd1a*$^{Del/+}$ macrophages. Most of the affected genes had a nearby GBS, suggesting that SETD1A mediates a significant part of GR's immunomodulatory actions.

We validated the specificity of our findings by reintroducing *Setd1a* into *Del* cells and were able to rescue *Dusp1* and *Tsc22d3* activation by overexpression of *Setd1a* (Figure 6G; Figure S6H). As the GR occupancy at those enhancers was not affected in *Del* cells (Figure S5D), the observed gene expression changes indeed resulted from impaired SETD1A function and not simply from loss of GR expression or binding.

In summary, we show that *Setd1a* is required for transcriptional control of specific innate immune responses mediated by GR and for activation of the interferon response downstream of TLR4 signaling in RAW264.7 cells.

GR-SETD1A target gene regulation in the absence of TLR4 signaling

Since our observations likely hint at a role for SETD1A downstream of TLR4 activation, which we did not fully investigate, we performed an RNA-seq experiment in RAW264.7 controls and mutants treated only with Dex, in the absence of LPS stimulation. Under these conditions, GR regulates a significantly different set of target genes (Figures 7A and 7B). While *Tsc22d3* and *Dusp1* are still induced, there is very little repression of inflammatory genes (such as *Cxcl10*, *Tnfa*, or *Il1a*, etc.) in macrophages treated only with Dex (compared with vehicle).

When comparing this response to ligand between control and *Setd1a* mutants, we found that several GR targets, such as *Dusp1* or *Il7r*, also showed differential expression upon SETD1A depletion in quiescent cells (Figure 7C). While GR target gene regulation was clearly affected in *Setd1a* mutants treated with Dex, the effect appears less pronounced and does not include as many inflammatory mediators (enriched GO terms "ossification" and "mononuclear cell migration") (Figures S7A and S7B).

Altogether, our data indicate that SETD1A is required for the transcriptional regulation of a subset of macrophage targets by GR, which is most prominent under inflammatory conditions.

DISCUSSION

Our genome-wide studies in LPS-activated macrophages revealed that GR interacts with the SETD1A/COMPASS complex to control the transcription of distinct subsets of
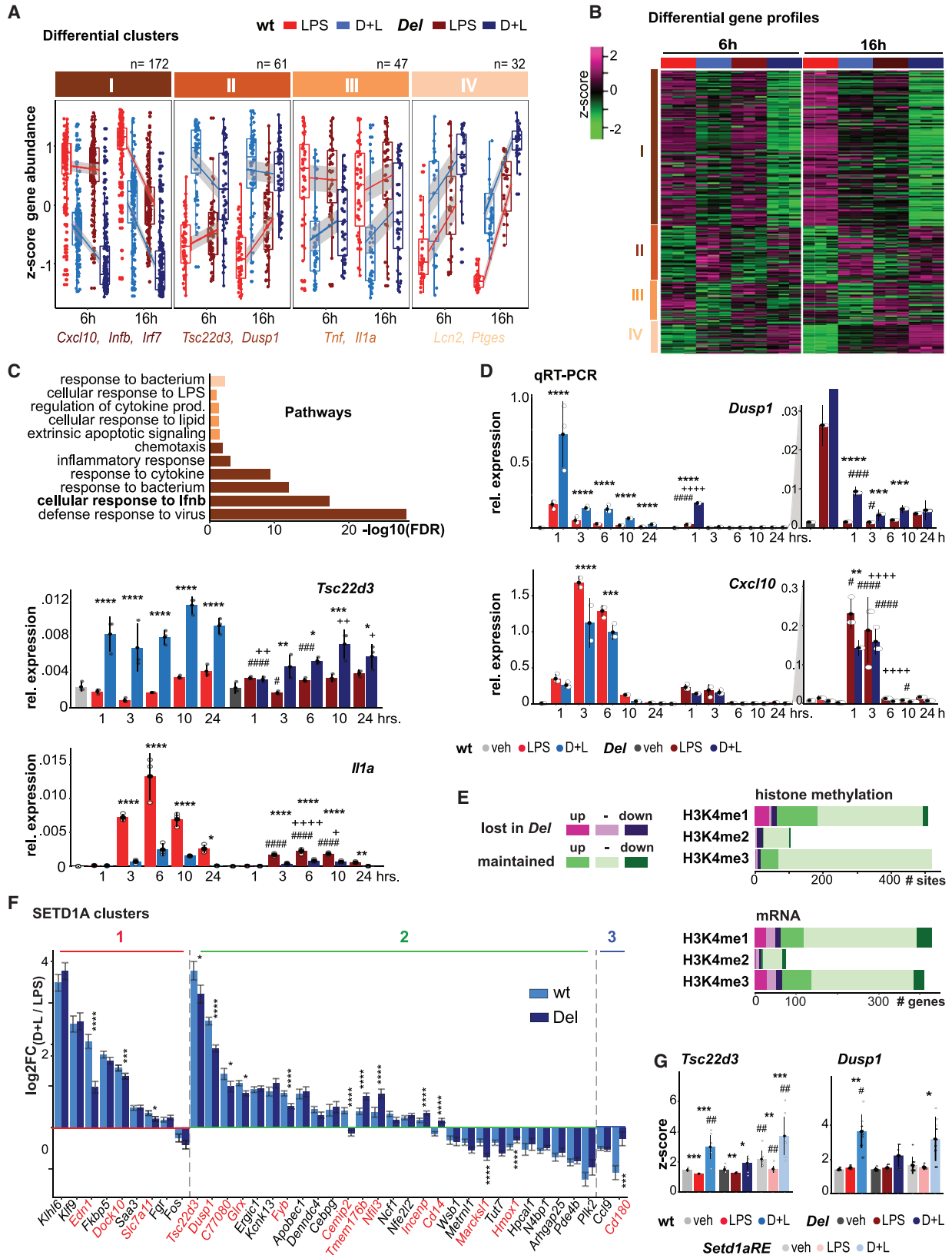
(legend on next page)

inflammatory gene networks. This interaction coincided with changes in H3K4me only at a limited number of specific loci, suggesting distinct *cis*-regulatory mechanisms exist at different enhancers. We characterized a mutant with unstable SETD1A protein and showed that *Setd1a* is required for a subset of GR-dependent gene regulation, but not for enhancer H3K4me.

Our observations of SETD1A/COMPASS enhancer occupancy agree with recent studies on accessible regions in erythrocytes and on MEF2-marked neuronal enhancers (van de Lagemaat et al., 2018; Mukai et al., 2019). These results challenge earlier views that SETD1A/COMPASS is exclusively recruited to promoters, as described in yeast and *Drosophila* (Ng et al., 2003; Ardehali et al., 2011). Conceivably, mammalian COMPASS family members acquired additional functions during their diversification, in line with increased genomic complexity. In addition to H3K4me, our data suggest SETD1A may exert additional transcriptional regulatory functions at distant sites, possibly independent of its H3K4 methyltransferase activity. Enhancer or promoter-specific factors might control the activity of SETD1A (Lee and Skalnik, 2008; Clouaire et al., 2012; Kim et al., 2013; Ebmeier et al., 2017; Hsu et al., 2019), for example, directing it to methylate non-histone proteins, as proposed for other SET-domain-containing complexes (Carlson and Gozani, 2016).

Recently, enhancer H3K4me2 was reported to inhibit GR binding in A549 cells (Clark et al., 2019). We did not detect a correlation between H3K4me2 and GR occupancy at the *Tsc22d3* and *Dusp1* enhancers, but we did observe reduced transcriptional activation of these genes in our *Setd1a* mutant (Figure 6; Figures S6D, 6G, 4C and 5B). Our results are consistent with the idea that H3K4me2 marks active transcription factor-binding regions in the genome (Wang et al., 2014). Nevertheless, locus- and cell-type-specific differences in H3K4me2 function may exist, as we observed that a certain fraction of GBSs gain H3K4me2 in response to Dex in macrophages. For instance, SETD1A recruitment co-occurs with increased H3K4me2 at the *Tsc22d3* locus, but not at other sites, emphasizing context-specific mechanisms for GR action.

For one of these subsets, we found that recruitment of SETD1A/COMPASS was linked to increased H3K27ac upon Dex + LPS stimulation in macrophages, indicating additive effects of SETD1A/COMPASS and HATs. A similar dependency of histone methyltransferases (HMTs) and P300 was previously seen for MLL4 and for GR-dependent G9a recruitment (Bittencourt et al., 2012; Wang et al., 2017). However, our ChIP experiments do not imply that SETD1A/COMPASS is required for HAT activity. On the contrary, P300 might potentially be required by GR to recruit SETD1A/COMPASS in response to ligand (Tang et al., 2013).

Unlike *set1* loss-of-function studies in *S. cerevisiae* (Schneider et al., 2005; Dehé et al., 2006; Kim et al., 2013), global H3K4me2/me3 was not abolished in our *Setd1a*$^{Del/+}$ cells. This suggests there may be redundancy between mammalian COMPASS complex family members. Also, the residual SETD1A or SETD1B proteins present in our *Del* cells could be sufficient to maintain di- and tri-methylation. Other HMTs could be compensating for depositing essential H3K4me3 at promoters (MLL1/2) and H3K4me2 at enhancers (MLL3/4) (Shilatifard, 2012; Meeks and Shilatifard, 2017). Nevertheless, we identified a number of differentially marked H3K4me1/me2/me3 sites, as well as thousands of differentially expressed *Setd1a*-dependent genes. These results suggest that distinct regulatory circuits are controlled by SETD1A/COMPASS, which differentially affect transcription dynamics and H3K4me patterns.

Moreover, we found COMPASS components co-enriched together with GR at hepatic *cis*-regulatory elements in mouse livers, and we measured transcriptional effects of SETD1A depletion in quiescent, Dex-treated macrophages without LPS stimulation. Conceivably, these findings might point toward additional roles for SETD1A as a GR coregulator in other conditions.

Taken together, we propose a model in which SETD1A is essential for the transcriptional control of GR-mediated inflammatory responses in a locus-specific manner, but which do not necessarily correlate with H3K4me or with H3K27ac. Our study shows that GR functions in a context- and locus-specific manner. For any given cell type or condition, different pioneer factors, cellular signals, neighboring transcription factors, epigenetic environments, and coregulators may shape the GC response. In order to develop novel immunomodulatory therapies and to reduce the adverse effects of anti-inflammatory GC treatment, all of these different mechanisms may need to be considered (Sacta et al., 2018; Clark et al., 2019).

Figure 6. SETD1A is required for the transcriptional regulation of certain myeloid GR targets

(A) Clustering of Dex-dependent genes affected by *Setd1a* deletion (weighted gene co-expression network analysis). The *Z*-standardized gene abundance of all genes per cluster is shown, with individual genes as single data points. The distribution median is the vertical line within the boxplot. Regression lines display transcriptional changes between WT and *Del* cells after LPS or Dex + LPS treatment (including a 95% confidence interval, gray shadow). n = cluster size, with example genes.

(B) *Setd1a*-dependent, Dex-regulated genes sorted by the log2FC in WT plus cluster membership (see A).

(C) GO biological process enrichment. Bar plots show −log10 of the FDR for each term (colors as in A).

(D) Time-series qRT-PCR, with mean relative expression as bars and standard deviation as error bars. n = 3, ANOVA with post hoc pairwise t test, Benjamini-Hochberg adj. *, treatment effect Dex + LPS over LPS; #, genotype effect compared with WT (LPS); +, genotype effect compared with WT (Dex + LPS).

(E) Bar plots classifying GR-SETD1A sites by significantly changed H3K4me1/me2/me3 (in response to ligand) and showing the number of sites with altered H3K4me1/me2/me3 (top, pink) or altered nearby transcripts in *Setd1a*$^{Del/+}$ cells (bottom, pink) (p < 0.05). Maintained regulation is shown in green, referring to Dex + LPS over LPS. −, invariant, unchanged.

(F) Log2FC of transcripts associated with GR-SETD1A sites classified in Figure 4B. Dex + LPS-treated WT and mutant cells were compared with LPS-treated samples. Error bars are log2 standard errors (n = 3, Wald test, Benjamini-Hochberg adj).

(G) qRT-PCR for GR targets in RAW264.7 cells re-expressing (RE) *Setd1a* in *Del* clones. Bars represent the means, and error bars represent the standard deviation. (n = 3, Kruskal-Wallis with post hoc pairwise Wilcoxon-Mann-Whitney test, Benjamini-Hochberg adj. *, treatment effect; #, genotype effect compared with *Del* cells). *p < 0.05, **p < 0.01, ***p < 0.001, ****p < 0.0001.
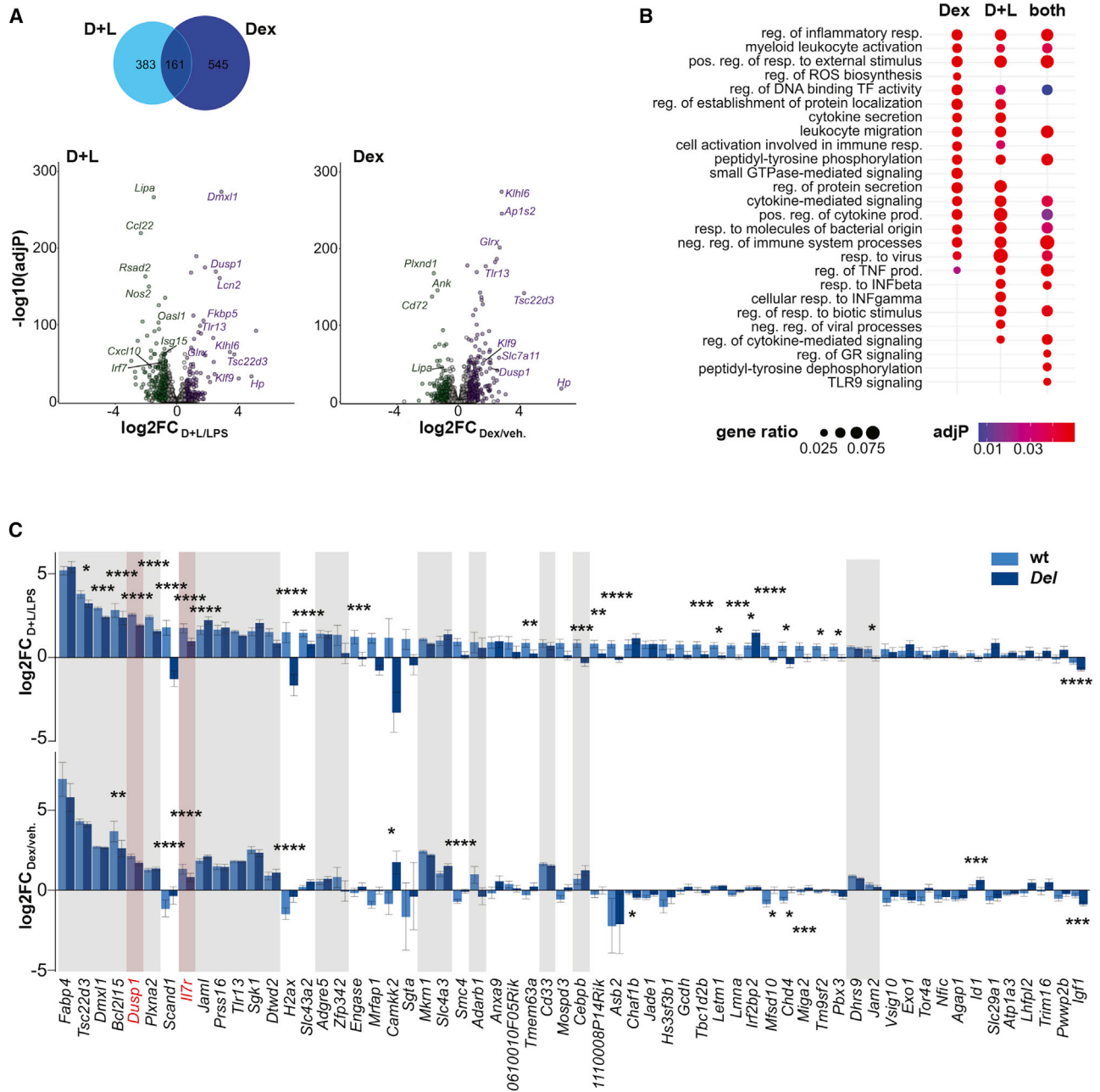
Figure 7. GR-SETD1A target gene regulation in the absence of TLR4 signaling

(A) Numbers of differentially expressed genes (Benjamini-Hochberg adj p < 0.05, FC > 1.5) in resting (Dex versus vehicle [veh]) and inflamed (Dex + LPS versus LPS) WT RAW264.7 cells (top). Volcano plots of transcriptional changes in Dex + LPS (over LPS)- and Dex (over veh)-treated cells (adj ps over log2 FCs). Purple, upregulated (adj p < 0.05, FC > 1.5); green, downregulated (adj p < 0.05, FC > 1.5) genes.

(B) Enrichment of GO biological pathways for genes exclusively regulated by Dex in resting (Dex) or in activated (D + L) macrophages, or in both.

(C) Comparison of the Dex response of cluster 2 (Figure 6A) in LPS-stimulated (D + L over LPS) and in untreated (Dex over veh) RAW264.7 cells. Bars, log2FC for WT and Setd1aDel/+ mutant cells; error bars, log2 standard error (Wald test, Benjamini-Hochberg-adjusted). Genes are sorted by their log2FC in WT LPS-treated cells. Gray shades: genes with similar responses to Dex in WT cells. Red shades: genes with impaired regulation in Del cells under both conditions. Benjamini-Hochberg adj p-values signify the genotype contribution to the Dex response (~genotype+treatment+treatment:genotype).

STAR★METHODS

Detailed methods are provided in the online version of this paper and include the following:

- KEY RESOURCES TABLE
- RESOURCE AVAILABILITY
  - Lead contact
  - Materials availability

REFERENCES

Ardehali, M.B., Mei, A., Zobeck, K.L., Caron, M., Lis, J.T., and Kusch, T. (2011). Drosophila Set1 is the major histone H3 lysine 4 trimethyltransferase with role in transcription. EMBO J. *30*, 2817–2828.

Bembom, O. (2019). seqLogo: Sequence logos for DNA sequence alignments. R package version R package version 1.34.0.

Beurton, F., Stempor, P., Caron, M., Appert, A., Dong, Y., Chen, R.A., Cluet, D., Couté, Y., Herbette, M., Huang, N., et al. (2019). Physical and functional inter-action between SET1/COMPASS complex component CFP-1 and a Sin3S HDAC complex in C. elegans. Nucleic Acids Res. *47*, 11164–11180.

Bian, C., Xu, C., Ruan, J., Lee, K.K., Burke, T.L., Tempel, W., Barsyte, D., Li, J., Wu, M., Zhou, B.O., et al. (2011). Sgf29 binds histone H3K4me2/3 and is required for SAGA complex recruitment and histone H3 acetylation. EMBO J. *30*, 2829–2842.

Bittencourt, D., Wu, D.Y., Jeong, K.W., Gerke, D.S., Herviou, L., Ianculescu, I., Chodankar, R., Siegmund, K.D., and Stallcup, M.R. (2012). G9a functions as a molecular scaffold for assembly of transcriptional coactivators on a subset of glucocorticoid receptor target genes. Proc. Natl. Acad. Sci. USA *109*, 19673–19678.

Bledau, A.S., Schmidt, K., Neumann, K., Hill, U., Ciotta, G., Gupta, A., Torres, D.C., Fu, J., Kranz, A., Stewart, A.F., and Anastassiadis, K. (2014). The H3K4 methyltransferase Setd1a is first required at the epiblast stage, whereas Setd1b becomes essential after gastrulation. Development *141*, 1022–1035.

Boa, S., Coert, C., and Patterton, H.G. (2003). Saccharomyces cerevisiae Set1p is a methyltransferase specific for lysine 4 of histone H3 and is required for efficient gene expression. Yeast *20*, 827–835.

Briggs, S.D., Bryk, M., Strahl, B.D., Cheung, W.L., Davie, J.K., Dent, S.Y., Winston, F., and Allis, C.D. (2001). Histone H3 lysine 4 methylation is mediated by Set1 and required for cell growth and rDNA silencing in Saccharomyces cerevisiae. Genes Dev. *15*, 3286–3295.

Brown, D.A., Di Cerbo, V., Feldmann, A., Ahn, J., Ito, S., Blackledge, N.P., Nakayama, M., McClellan, M., Dimitrova, E., Turberfield, A.H., et al. (2017). The SET1 Complex Selects Actively Transcribed Target Genes via Multivalent Interaction with CpG Island Chromatin. Cell Rep. *20*, 2313–2327.

Carlson, S.M., and Gozani, O. (2016). Nonhistone Lysine Methylation in the Regulation of Cancer Pathways. Cold Spring Harb. Perspect. Med. *6*, a026435.

Chen, W., and Roeder, R.G. (2007). The Mediator subunit MED1/TRAP220 is required for optimal glucocorticoid receptor-mediated transcription activation. Nucleic Acids Res. *35*, 6161–6169.

Chinenov, Y., Sacta, M.A., Cruz, A.R., and Rogatsky, I. (2008). GRIP1-associated SET-domain methyltransferase in glucocorticoid receptor target gene expression. Proc. Natl. Acad. Sci. USA *105*, 20185–20190.

Clark, E.A., Wu, F., Chen, Y., Kang, P., Kaiser, U.B., Fang, R., and Shi, Y.G. (2019). GR and LSD1/KDM1A-Targeted Gene Activation Requires Selective H3K4me2 Demethylation at Enhancers. Cell Rep. *27*, 3522–3532.e3.

Clouaire, T., Webb, S., Skene, P., Illingworth, R., Kerr, A., Andrews, R., Lee, J.H., Skalnik, D., and Bird, A. (2012). Cfp1 integrates both CpG content and gene activity for accurate H3K4me3 deposition in embryonic stem cells. Genes Dev. *26*, 1714–1728.

Couture, J.F., and Skiniotis, G. (2013). Assembling a COMPASS. Epigenetics *8*, 349–354.

Cox, J., and Mann, M. (2008). MaxQuant enables high peptide identification rates, individualized p.p.b.-range mass accuracies and proteome-wide protein quantification. Nat. Biotechnol. *26*, 1367–1372.

Creyghton, M.P., Cheng, A.W., Welstead, G.G., Kooistra, T., Carey, B.W., Steine, E.J., Hanna, J., Lodato, M.A., Frampton, G.M., Sharp, P.A., et al. (2010). Histone H3K27ac separates active from poised enhancers and predicts developmental state. Proc. Natl. Acad. Sci. USA *107*, 21931–21936.

Cunningham, F., Achuthan, P., Akanni, W., Allen, J., Amode, M.R., Armean, I.M., Bennett, R., Bhai, J., Billis, K., Boddu, S., et al. (2019). Ensembl 2019. Nucleic Acids Res. *47* (*D1*), D745–D751.

Dehé, P.M., Dichtl, B., Schaft, D., Roguev, A., Pamblanco, M., Lebrun, R., Rodríguez-Gil, A., Mkandawire, M., Landsberg, K., Shevchenko, A., et al. (2006). Protein interactions within the Set1 complex and their roles in the regulation of histone 3 lysine 4 methylation. J. Biol. Chem. *281*, 35404–35412.

Dorighi, K.M., Swigut, T., Henriques, T., Bhanu, N.V., Scruggs, B.S., Nady, N., Still, C.D., 2nd, Garcia, B.A., Adelman, K., and Wysocka, J. (2017). Mll3 and Mll4 Facilitate Enhancer RNA Synthesis and Transcription from Promoters Independently of H3K4 Monomethylation. Mol. Cell *66*, 568–576.e4.

Durinck, S., Spellman, P.T., Birney, E., and Huber, W. (2009). Mapping identifiers for the integration of genomic datasets with the R/Bioconductor package biomaRt. Nat. Protoc. *4*, 1184–1191.

Dynan, W.S., and Tjian, R. (1983). The promoter-specific transcription factor Sp1 binds to upstream sequences in the SV40 early promoter. Cell *35*, 79–87.

Ebmeier, C.C., Erickson, B., Allen, B.L., Allen, M.A., Kim, H., Fong, N., Jacobsen, J.R., Liang, K., Shilatifard, A., Dowell, R.D., et al. (2017). Human TFIIH Kinase CDK7 Regulates Transcription-Associated Chromatin Modifications. Cell Rep. *20*, 1173–1186.

Eden, E., Navon, R., Steinfeld, I., Lipson, D., and Yakhini, Z. (2009). GOrilla: a tool for discovery and visualization of enriched GO terms in ranked gene lists. BMC Bioinformatics *10*, 48.

Egan, B., Yuan, C.C., Craske, M.L., Labhart, P., Guler, G.D., Arnott, D., Maile, T.M., Busby, J., Henry, C., Kelly, T.K., et al. (2016). An Alternative Approach to ChIP-Seq Normalization Enables Detection of Genome-Wide Changes in Histone H3 Lysine 27 Trimethylation upon EZH2 Inhibition. PLoS ONE *11*, e0166438.

Escoter-Torres, L., Caratti, G., Mechtidou, A., Tuckermann, J., Uhlenhaut, N.H., and Vettorazzi, S. (2019). Fighting the Fire: Mechanisms of Inflammatory Gene Regulation by the Glucocorticoid Receptor. Front. Immunol. *10*, 1859.

Freese, N.H., Norris, D.C., and Loraine, A.E. (2016). Integrated genome browser: visual analytics platform for genomics. Bioinformatics *32*, 2089–2095.

Greulich, F., Hemmer, M.C., Rollins, D.A., Rogatsky, I., and Uhlenhaut, N.H. (2016). There goes the neighborhood: Assembly of transcriptional complexes during the regulation of metabolism and inflammation by the glucocorticoid receptor. Steroids *114*, 7–15.

Grøntved, L., John, S., Baek, S., Liu, Y., Buckley, J.R., Vinson, C., Aguilera, G., and Hager, G.L. (2013). C/EBP maintains chromatin accessibility in liver and facilitates glucocorticoid receptor recruitment to steroid response elements. EMBO J. *32*, 1568–1583.

Gross, K.L., and Cidlowski, J.A. (2008). Tissue-specific glucocorticoid action: a family affair. Trends Endocrinol. Metab. *19*, 331–339.

Heigwer, F., Kerr, G., and Boutros, M. (2014). E-CRISP: fast CRISPR target site identification. Nat. Methods *11*, 122–123.

Heinz, S., Benner, C., Spann, N., Bertolino, E., Lin, Y.C., Laslo, P., Cheng, J.X., Murre, C., Singh, H., and Glass, C.K. (2010). Simple combinations of lineage-determining transcription factors prime cis-regulatory elements required for macrophage and B cell identities. Mol. Cell *38*, 576–589.

Hemmer, M.C., Wierer, M., Schachtrup, K., Downes, M., Hübner, N., Evans, R.M., and Uhlenhaut, N.H. (2019). E47 modulates hepatic glucocorticoid action. Nat. Commun. *10*, 306.

Hsu, P.L., Shi, H., Leonen, C., Kang, J., Chatterjee, C., and Zheng, N. (2019). Structural Basis of H2B Ubiquitination-Dependent H3K4 Methylation by COMPASS. Mol. Cell *76*, 712–723.e4.

Hua, G., Ganti, K.P., and Chambon, P. (2016). Glucocorticoid-induced tethered transrepression requires SUMOylation of GR and formation of a SUMO-SMRT/NCoR1-HDAC3 repressing complex. Proc. Natl. Acad. Sci. USA *113*, E635–E643.

Ito, K., Barnes, P.J., and Adcock, I.M. (2000). Glucocorticoid receptor recruitment of histone deacetylase 2 inhibits interleukin-1beta-induced histone H4 acetylation on lysines 8 and 12. Mol. Cell. Biol. *20*, 6891–6903.

Jang, Y., Wang, C., Zhuang, L., Liu, C., and Ge, K. (2017). H3K4 Methyltransferase Activity Is Required for MLL4 Protein Stability. J. Mol. Biol. *429*, 2046–2054.

John, S., Sabo, P.J., Thurman, R.E., Sung, M.H., Biddie, S.C., Johnson, T.A., Hager, G.L., and Stamatoyannopoulos, J.A. (2011). Chromatin accessibility pre-determines glucocorticoid receptor binding patterns. Nat. Genet. *43*, 264–268.

Jonat, C., Rahmsdorf, H.J., Park, K.K., Cato, A.C., Gebel, S., Ponta, H., and Herrlich, P. (1990). Antitumor promotion and antiinflammation: down-modulation of AP-1 (Fos/Jun) activity by glucocorticoid hormone. Cell *62*, 1189–1204.

Kaikkonen, M.U., Spann, N.J., Heinz, S., Romanoski, C.E., Allison, K.A., Stender, J.D., Chun, H.B., Tough, D.F., Prinjha, R.K., Benner, C., and Glass, C.K. (2013). Remodeling of the enhancer landscape during macrophage activation is coupled to enhancer transcription. Mol. Cell *51*, 310–325.

Khan, A., Fornes, O., Stigliani, A., Gheorghe, M., Castro-Mondragon, J.A., van der Lee, R., Bessy, A., Chèneby, J., Kulkarni, S.R., Tan, G., et al. (2018). JASPAR 2018: update of the open-access database of transcription factor binding profiles and its web framework. Nucleic Acids Res. *46* (*D1*), D1284.

Kim, J., Kim, J.A., McGinty, R.K., Nguyen, U.T., Muir, T.W., Allis, C.D., and Roeder, R.G. (2013). The n-SET domain of Set1 regulates H2B ubiquitylation-dependent H3K4 methylation. Mol. Cell *49*, 1121–1133.

Kino, T., Nordeen, S.K., and Chrousos, G.P. (1999). Conditional modulation of glucocorticoid receptor activities by CREB-binding protein (CBP) and p300. J. Steroid Biochem. Mol. Biol. *70*, 15–25.

Kulakovskiy, I.V., Vorontsov, I.E., Yevshin, I.S., Sharipov, R.N., Fedorova, A.D., Rumynskiy, E.I., Medvedeva, Y.A., Magana-Mora, A., Bajic, V.B., Papatsenko, D.A., et al. (2018). HOCOMOCO: towards a complete collection of transcription factor binding models for human and mouse via large-scale ChIP-Seq analysis. Nucleic Acids Res. *46* (*D1*), D252–D259.

Lawrence, M., Huber, W., Pagès, H., Aboyoun, P., Carlson, M., Gentleman, R., Morgan, M.T., and Carey, V.J. (2013). Software for computing and annotating genomic ranges. PLoS Comput. Biol. *9*, e1003118.

Lee, J.H., and Skalnik, D.G. (2005). CpG-binding protein (CXXC finger protein 1) is a component of the mammalian Set1 histone H3-Lys4 methyltransferase complex, the analogue of the yeast Set1/COMPASS complex. J. Biol. Chem. *280*, 41725–41731.

Lee, J.H., and Skalnik, D.G. (2008). Wdr82 is a C-terminal domain-binding protein that recruits the Setd1A Histone H3-Lys4 methyltransferase complex to transcription start sites of transcribed human genes. Mol. Cell. Biol. *28*, 609–618.

Li, H. (2013). Aligning sequence reads, clone sequences and assembly contigs with BWA-MEM. arXiv, 13033997. https://arxiv.org/abs/1303.3997.

Li, H., Ilin, S., Wang, W., Duncan, E.M., Wysocka, J., Allis, C.D., and Patel, D.J. (2006). Molecular basis for site-specific read-out of histone H3K4me3 by the BPTF PHD finger of NURF. Nature *442*, 91–95.

Li, H., Handsaker, B., Wysoker, A., Fennell, T., Ruan, J., Homer, N., Marth, G., Abecasis, G., and Durbin, R.; 1000 Genome Project Data Processing Subgroup (2009). The Sequence Alignment/Map format and SAMtools. Bioinformatics *25*, 2078–2079.

Love, M.I., Huber, W., and Anders, S. (2014). Moderated estimation of fold change and dispersion for RNA-seq data with DESeq2. Genome Biol. *15*, 550.

Machanick, P., and Bailey, T.L. (2011). MEME-ChIP: motif analysis of large DNA datasets. Bioinformatics *27*, 1696–1697.

McLean, C.Y., Bristor, D., Hiller, M., Clarke, S.L., Schaar, B.T., Lowe, C.B., Wenger, A.M., and Bejerano, G. (2010). GREAT improves functional interpretation of cis-regulatory regions. Nat. Biotechnol. *28*, 495–501.

Meeks, J.J., and Shilatifard, A. (2017). Multiple Roles for the MLL/COMPASS Family in the Epigenetic Regulation of Gene Expression and in Cancer. Annu. Rev. Cancer Biol. *1*, 425–446.

Mukai, J., Cannavò, E., Crabtree, G.W., Sun, Z., Diamantopoulou, A., Thakur, P., Chang, C.Y., Cai, Y., Lomvardas, S., Takata, A., et al. (2019). Recapitulation and Reversal of Schizophrenia-Related Phenotypes in Setd1a-Deficient Mice. Neuron *104*, 471–487.e12.

Nagy, P.L., Griesenbeck, J., Kornberg, R.D., and Cleary, M.L. (2002). A trithorax-group complex purified from Saccharomyces cerevisiae is required for methylation of histone H3. Proc. Natl. Acad. Sci. USA *99*, 90–94.

Nathan, C., and Ding, A. (2010). Nonresolving inflammation. Cell *140*, 871–882.

Nelson, J.D., Denisenko, O., and Bomsztyk, K. (2006). Protocol for the fast chromatin immunoprecipitation (ChIP) method. Nat. Protoc. *1*, 179–185.

Newburger, D.E., and Bulyk, M.L. (2009). UniPROBE: an online database of protein binding microarray data on protein-DNA interactions. Nucleic Acids Res. *37*, D77–D82.

Ng, H.H., Robert, F., Young, R.A., and Struhl, K. (2003). Targeted recruitment of Set1 histone methylase by elongating Pol II provides a localized mark and memory of recent transcriptional activity. Mol. Cell *11*, 709–719.

Oakley, R.H., and Cidlowski, J.A. (2013). The biology of the glucocorticoid receptor: new signaling mechanisms in health and disease. J. Allergy Clin. Immunol. *132*, 1033–1044.

Pachkov, M., Balwierz, P.J., Arnold, P., Ozonov, E., and van Nimwegen, E. (2013). SwissRegulon, a database of genome-wide annotations of regulatory sites: recent updates. Nucleic Acids Res. *41*, D214–D220.

Patro, R., Duggal, G., Love, M.I., Irizarry, R.A., and Kingsford, C. (2017). Salmon provides fast and bias-aware quantification of transcript expression. Nat. Methods *14*, 417–419.

Pekowska, A., Benoukraf, T., Zacarias-Cabeza, J., Belhocine, M., Koch, F., Holota, H., Imbert, J., Andrau, J.C., Ferrier, P., and Spicuglia, S. (2011). H3K4 tri-methylation provides an epigenetic signature of active enhancers. EMBO J. *30*, 4198–4210.

Postic, C., Shiota, M., Niswender, K.D., Jetton, T.L., Chen, Y., Moates, J.M., Shelton, K.D., and Lindner, J. (1999 Jan 1). A D: "Dual roles for glucokinase in glucose homeostasis as determined by liver and pancreatic beta cell-specific gene knock-outs using Cre recombinase". J. Biol. Chem. *274*, 305-15. https://doi.org/10.1074/jbc.274.1.305.

Quagliarini, F., Mir, A.A., Balazs, K., Wierer, M., Dyar, K.A., Jouffe, C., Makris, K., Hawe, J., Heinig, M., Filipp, F.V., et al. (2019). Cistromic Reprogramming of the Diurnal Glucocorticoid Hormone Response by High-Fat Diet. Mol. Cell *76*, 531–545.e5.

Quinlan, A.R., and Hall, I.M. (2010). BEDTools: a flexible suite of utilities for comparing genomic features. Bioinformatics *26*, 841–842.

Ramírez, F., Ryan, D.P., Grüning, B., Bhardwaj, V., Kilpert, F., Richter, A.S., Heyne, S., Dündar, F., and Manke, T. (2016). deepTools2: a next generation web server for deep-sequencing data analysis. Nucleic Acids Res. *44 (W1)*, W160–W165.

Ray, A., and Prefontaine, K.E. (1994). Physical association and functional antagonism between the p65 subunit of transcription factor NF-kappa B and the glucocorticoid receptor. Proc. Natl. Acad. Sci. USA *91*, 752–756.

R Core Team (2017). R: A Language and Environment for Statistical Computing (R Foundation for Statistical Computing).

Rollins, D.A., Kharlyngdoh, J.B., Coppo, M., Tharmalingam, B., Mimouna, S., Guo, Z., Sacta, M.A., Pufall, M.A., Fisher, R.P., Hu, X., et al. (2017). Glucocorticoid-induced phosphorylation by CDK9 modulates the coactivator functions of transcriptional cofactor GRIP1 in macrophages. Nat. Commun. *8*, 1739.

Sacta, M.A., Tharmalingam, B., Coppo, M., Rollins, D.A., Deochand, D.K., Benjamin, B., Yu, L., Zhang, B., Hu, X., Li, R., et al. (2018). Gene-specific mechanisms direct glucocorticoid-receptor-driven repression of inflammatory response genes in macrophages. eLife *7*, e34864.

Santos-Rosa, H., Schneider, R., Bannister, A.J., Sherriff, J., Bernstein, B.E., Emre, N.C., Schreiber, S.L., Mellor, J., and Kouzarides, T. (2002). Active genes are tri-methylated at K4 of histone H3. Nature *419*, 407–411.

Schneider, J., Wood, A., Lee, J.S., Schuster, R., Dueker, J., Maguire, C., Swanson, S.K., Florens, L., Washburn, M.P., and Shilatifard, A. (2005). Molecular regulation of histone H3 trimethylation by COMPASS and the regulation of gene expression. Mol. Cell *19*, 849–856.

Scrucca, L., Fop, M., Murphy, T.B., and Raftery, A.E. (2016). mclust 5: Clustering, Classification and Density Estimation Using Gaussian Finite Mixture Models. R J. *8*, 289–317.

Shilatifard, A. (2012). The COMPASS family of histone H3K4 methylases: mechanisms of regulation in development and disease pathogenesis. Annu. Rev. Biochem. *81*, 65–95.

Sims, R.J., 3rd, Millhouse, S., Chen, C.F., Lewis, B.A., Erdjument-Bromage, H., Tempst, P., Manley, J.L., and Reinberg, D. (2007). Recognition of trimethylated histone H3 lysine 4 facilitates the recruitment of transcription postinitiation factors and pre-mRNA splicing. Mol. Cell *28*, 665–676.

Soares, L.M., Radman-Livaja, M., Lin, S.G., Rando, O.J., and Buratowski, S. (2014). Feedback control of Set1 protein levels is important for proper H3K4 methylation patterns. Cell Rep. *6*, 961–972.

Soares, L.M., He, P.C., Chun, Y., Suh, H., Kim, T., and Buratowski, S. (2017). Determinants of Histone H3K4 Methylation Patterns. Mol. Cell *68*, 773–785.e6.

Soneson, C., Love, M.I., and Robinson, M.D. (2015). Differential analyses for RNA-seq: transcript-level estimates improve gene-level inferences. F1000Res. *4*, 1521.

Strähle, U., Klock, G., and Schütz, G. (1987). A DNA sequence of 15 base pairs is sufficient to mediate both glucocorticoid and progesterone induction of gene expression. Proc. Natl. Acad. Sci. USA *84*, 7871–7875.

Tang, Z., Chen, W.Y., Shimada, M., Nguyen, U.T., Kim, J., Sun, X.J., Sengoku, T., McGinty, R.K., Fernandez, J.P., Muir, T.W., and Roeder, R.G. (2013). SET1

and p300 act synergistically, through coupled histone modifications, in transcriptional activation by p53. Cell *154*, 297–310.

Tronche, F., Kellendonk, C., Kretz, O., Gass, P., Anlag, K., Orban, P.C., Bock, R., Klein, R., and Schütz, G. (1999 Sep). Disruption of the glucocorticoid receptor gene in the nervous system results in reduced anxiety. Nat Genet *23*, 99–103. https://doi.org/10.1038/12703.

Turvey, S.E., and Broide, D.H. (2010). Innate immunity. J. Allergy Clin. Immunol. *125 (2, Suppl 2)*, S24–S32.

Tusi, B.K., Deng, C., Salz, T., Zeumer, L., Li, Y., So, C.W., Morel, L.M., Qiu, Y., and Huang, S. (2015). Setd1a regulates progenitor B-cell-to-precursor B-cell development through histone H3 lysine 4 trimethylation and Ig heavy-chain rearrangement. FASEB J. *29*, 1505–1515.

Tyanova, S., and Cox, J. (2018). Perseus: A Bioinformatics Platform for Integrative Analysis of Proteomics Data in Cancer Research. Methods Mol. Biol. *1711*, 133–148.

Uhlenhaut, N.H., Barish, G.D., Yu, R.T., Downes, M., Karunasiri, M., Liddle, C., Schwalie, P., Hübner, N., and Evans, R.M. (2013). Insights into negative regulation by the glucocorticoid receptor from genome-wide profiling of inflammatory cistromes. Mol. Cell *49*, 158–171.

van de Lagemaat, L.N., Flenley, M., Lynch, M.D., Garrick, D., Tomlinson, S.R., Kranc, K.R., and Vernimmen, D. (2018). CpG binding protein (CFP1) occupies open chromatin regions of active genes, including enhancers and non-CpG islands. Epigenetics Chromatin *11*, 59.

Vermeulen, M., Mulder, K.W., Denissov, S., Pijnappel, W.W., van Schaik, F.M., Varier, R.A., Baltissen, M.P., Stunnenberg, H.G., Mann, M., and Timmers, H.T. (2007). Selective anchoring of TFIID to nucleosomes by trimethylation of histone H3 lysine 4. Cell *131*, 58–69.

Wang, W., Guo, C., Li, W., Li, J., Wang, W., Myatt, L., and Sun, K. (2012). Involvement of GR and p300 in the induction of H6PD by cortisol in human amnion fibroblasts. Endocrinology *153*, 5993–6002.

Wang, Y., Li, X., and Hu, H. (2014). H3K4me2 reliably defines transcription factor binding regions in different cells. Genomics *103*, 222–228.

Wang, S.P., Tang, Z., Chen, C.W., Shimada, M., Koche, R.P., Wang, L.H., Nakadai, T., Chramiec, A., Krivtsov, A.V., Armstrong, S.A., and Roeder, R.G. (2017). A UTX-MLL4-p300 Transcriptional Regulatory Network Coordinately Shapes Active Enhancer Landscapes for Eliciting Transcription. Mol. Cell *67*, 308–321.e6.

Wickham, H. (2016). Elegant Graphics for Data Analysis (Springer-Verlag).

Wu, M., Wang, P.F., Lee, J.S., Martin-Brown, S., Florens, L., Washburn, M., and Shilatifard, A. (2008). Molecular regulation of H3K4 trimethylation by Wdr82, a component of human Set1/COMPASS. Mol. Cell. Biol. *28*, 7337–7344.

Wysocka, J., Swigut, T., Xiao, H., Milne, T.A., Kwon, S.Y., Landry, J., Kauer, M., Tackett, A.J., Chait, B.T., Badenhorst, P., et al. (2006). A PHD finger of NURF couples histone H3 lysine 4 trimethylation with chromatin remodelling. Nature *442*, 86–90.

Yang, W., and Ernst, P. (2017). SET/MLL family proteins in hematopoiesis and leukemia. Int. J. Hematol. *105*, 7–16.

Yang-Yen, H.F., Chambard, J.C., Sun, Y.L., Smeal, T., Schmidt, T.J., Drouin, J., and Karin, M. (1990). Transcriptional interference between c-Jun and the glucocorticoid receptor: mutual inhibition of DNA binding due to direct protein-protein interaction. Cell *62*, 1205–1215.

Yu, G., Wang, L.G., Han, Y., and He, Q.Y. (2012). clusterProfiler: an R package for comparing biological themes among gene clusters. OMICS *16*, 284–287.

Zhang, Y., Liu, T., Meyer, C.A., Eeckhoute, J., Johnson, D.S., Bernstein, B.E., Nusbaum, C., Myers, R.M., Brown, M., Li, W., and Liu, X.S. (2008). Model-based analysis of ChIP-Seq (MACS). Genome Biol. *9*, R137.

Zhang, T., Zhang, Z., Dong, Q., Xiong, J., and Zhu, B. (2020). Histone H3K27 acetylation is dispensable for enhancer activity in mouse embryonic stem cells. Genome Biol. *21*, 45.

Zhu, L.J., Gazin, C., Lawson, N.D., Pagès, H., Lin, S.M., Lapointe, D.S., and Green, M.R. (2010). ChIPpeakAnno: a Bioconductor package to annotate ChIP-seq and ChIP-chip data. BMC Bioinformatics *11*, 237.

STAR★METHODS

KEY RESOURCES TABLE

REAGENT or RESOURCE	SOURCE	IDENTIFIER
Antibodies		
Rabbit polyclonal anti-betaTubulin	Santa Cruz Biotechnology	Cat.#sc-9104; RRID:AB_2241191
Mouse monoclonal anti-CXXC1	Santa Cruz Biotechnology	Cat.#sc-136419
Mouse monoclonal anti-GR	Santa Cruz Biotechnology	Cat.#sc-393232; RRID:AB_2687823
Rabbit polyclonal anti-H3	Abcam	Cat.#ab1791; RRID:AB_302613
Mouse monoclonal anti-H3K4me1	Diagenode	Cat.#C15200150
Mouse monoclonal anti-H3K4me2	Diagenode	Cat.#C15200151
Mouse monoclonal anti-H3K4me3	Diagenode	Cat.#C15200152
Goat anti-mouse IgG (HRP-conjugated)	Bio-Rad	Cat.#170-6516; RRID:AB_11125547
Donkey anti-mouse IgG (IRDye680LT)	Li-Cor	Cat.#926-68022; RRID:AB_10715072
Goat anti-rabbit IgG (HRP-conjugated)	Dianova	Cat.#111-035-003; RRID:AB_2313567
Donkey anti-rabbit IgG (IRDye800CW)	Li-Cor	Cat.#926-32213; RRID:AB_621848
Mouse monoclonal anti-SETD1A	Thermo Fisher Scientific	Cat.#MA5-26764; RRID:AB_2725334
Rabbit monoclonal anti-WDR82	Cell Signaling Technology	Cat.#99715; RRID:AB_2800319
Rabbit polyclonal anti-CXXC1	Abcam	Cat.#ab198977
Rabbit polyclonal anti-GR	Protein Tech	Cat.#24050-1-AP; RRID:AB_2813890
Rabbit polyclonal anti-H3	Abcam	Cat.#ab1791; RRID:AB_302613
Rabbit polyclonal anti-H3K27Ac	Abcam	Cat.#ab4729; RRID:AB_2118291
Rabbit polyclonal anti-H3K4me1	Diagenode	Cat.#C15410194; RRID:AB_2637078
Rabbit polyclonal anti-H3K4me2	Abcam	Cat.#ab7766; RRID:AB_2560996
Rabbit polyclonal anti-H3K4me3	Millipore/Merck	Cat.#05-745R; RRID:AB_1587134
Normal rabbit IgG	Cell Signaling Technology	Cat.#2729; RRID:AB_1031062
Rabbit polyclonal anti-SET1	Bethyl	Cat.#A300-289A; RRID:AB_263413
WDR82	Cell Signaling Technology	Cat.#99715; RRID:AB_2800319
Bacterial and virus strains		
Biological Samples		
Chemicals, peptides, and recombinant proteins		
cOmplete, Mini, EDTA-free Protease-Inhibitor-Cocktail	Roche	Cat.#11836170001
cOmplete-Ultra, EDTA-free Protease Inhibitor Cocktail	Roche	Cat.#5892953001
Ficoll Paque PLUS	GE Healthcare	Cat.#17144002
DMEM (4.5 g/L glucose)	Sigma	Cat.#D6429-500
Fetal Bovine Serum	Sigma	Cat.#F9665
Fetal Bovine Serum, dyalized	Sigma	Cat.#F0392-100ml
dexamethasone	Sigma	Cat.#D4902
LPS E.COLI O111:B4	Sigma	Cat.#LPS25
Interferon-beta1	R&D Systems	Cat.#8234-MB-010
Dynabeads M-280 Sheep Anti-Rabbit IgG	Life Technologies	Cat.#11204D
Sepharose Protein A/G	Rockland	Cat.#PAG50-00-0002
DSG Crosslinker	Proteochem	Cat.#C1104
16% Formaldehyde (w/v), Methanol-free	Thermo Scientific	Cat.#28906
Power Sybr Green Mastermix	Thermo Scientific	Cat.#4367659

(Continued on next page)

Continued

REAGENT or RESOURCE	SOURCE	IDENTIFIER
Gel Cassettes, Pippin Prep, dye-free	Sage Science	Cat.#CDF2010
4-12% Bis-Tris SDS-PAGE gel	Life Technologies	Cat.#NP0323BOX
Agencourt® AMPure® XP	Beckman Coulter GmbH	Cat.#A63881
Critical commercial assays		
RNeasy Mini Kit for RNA extraction	QIAGEN	Cat.#74106
MinElute PCR purification kit	QIAGEN	Cat.#28006
Kapa Hyper Prep	Roche	Cat.#7962363001
Lib Quant Illumina Rox Low	Roche	Cat.#7960336001
RNA 6000 Nano Kit	Agilent Technologies	Cat.#5067-1511
High Sensitivity DNA Kit	Agilent Technologies	Cat.#5067-4626
QuantiTect Reverse Transcription kit	QIAGEN	Cat.#205314
Neon Transfection System 10 µL Kit-25 x	Life Technologies	Cat.# MPK1025
Qubit dsDNA HS Assay Kit	Life Technologies	Cat.#Q32854
Deposited data		
ChIP-MS	This paper	PRIDE:PXD018077
ChIP-Seq in macrophages	This paper	GEO:GSE136070
GR ChIP-Seq in macrophages	This paper	GEO:GSM1446192
GR ChIP-Seq in macrophages	This paper	GEO:GSM788651
ChIP-Seq in RAW264.7	This paper	GEO:GSE138017
RNA-Seq in wildtype macrophages	This paper	GEO:GSE137412
RNA-Seq in RAW264.7 cells (wildtype and *Setd1a*$^{Del/+}$) and *Setd1bKO* macrophages	This paper	GEO:GSE137944
Experimental models: cell lines		
RAW264.7	ATCC	Cat.#TIB-71 ; RRID:CVCL_0493
RAW264.7 *Setd1a*$^{Del/+}$	This paper	
S2 cells (*Drosophila*)	provided by Prof. P. Becker (LMU Munich, Germany)	RRID:CVCL_Z232
Experimental models: organisms/strains		
Speer6-ps1$^{Tg(Alb-cre)21Mgn}$	Postic et al., 1999	
Nr3c1^{tm2Gsc}/*Nr3c1*^{tm2Gsc}	Tronche et al., 1999	RRID:MGI:6257049
Setd1b$^{tm1.3Afst}$/*Setd1b*$^{tm1.3Afst}$	provided by Prof. Dr. K. Anastassiadis (TU Dresden, Germany) Bledau et al., 2014	RRID:MGI:5568956
Setd1a$^{tm1.2Afst}$/*Setd1a*$^{tm1.2Afst}$	provided by Prof. Dr. K. Anastassiadis (TU Dresden, Germany) Bledau et al., 2014	RRID:MGI:5568947
Rosa26-Cre-ERT2 (RC)	provided by Prof. Dr. K. Anastassiadis (TU Dresden, Germany) Bledau et al., 2014	
Oligonucleotides		
See Table S6		
Recombinant DNA		
pU6.chimeric	gift from I. Burtscher, Helmholtz Zentrum Muenchen	
pCAG.Cas9D10A-EGFP	gift from I. Burtscher, Helmholtz Zentrum Muenchen	
pPB-Puro-mPGK-EGFP:3xGGGGS:mSetd1a	This paper, VectorBuilder	

(Continued on next page)

Continued

REAGENT or RESOURCE	SOURCE	IDENTIFIER
Software and algorithms		
Perseus v.1.5.1.1	Tyanova and Cox, 2018	RRID:SCR_015753; https://maxquant.net/perseus/
MaxQuant v1.5.1.1	Cox and Mann, 2008	RRID:SCR_014485; https://maxquant.net/maxquant/
GOrilla	Eden et al., 2009	RRID:SCR_006848; http://cbl-gorilla.cs.technion.ac.il/
FastQC	http://www.bioinformatics.babraham.ac.uk/projects/fastqc/	RRID:SCR_014583
Salmon v0.10.2	Patro et al., 2017	RRID:SCR_017036; https://combine-lab.github.io/salmon/
R v3.6.1	R Core Team, 2017	RRID:SCR_001905; https://cran.r-project.org/
DESeq2 v1.22.0	Love et al., 2014	RRID:SCR_015687; https://bioconductor.org/packages/release/bioc/html/DESeq2.html
tximport	Soneson et al., 2015	RRID:SCR_016752; https://bioconductor.org/packages/release/bioc/html/tximport.html
GenomicRanges v1.36.1	Lawrence et al., 2013	RRID:SCR_000025; https://bioconductor.org/packages/release/bioc/html/GenomicRanges.html
ggplot2 v3.2.1	Wickham, 2016	RRID:SCR_014601; https://cran.r-project.org/web/packages/ggplot2/index.html
gplots v3.0.1.1	https://github.com/talgalili/gplots/	
ChIPpeakAnno v3.18.2	Zhu et al., 2010	RRID:SCR_012828; https://bioconductor.org/packages/release/bioc/html/ChIPpeakAnno.html
biomaRt v2.38	Durinck et al., 2009	RRID:SCR_002987; https://bioconductor.org/packages/release/bioc/html/biomaRt.html
Clusterprofiler v3.16.1	Yu et al., 2012	RRID:SCR_016884; https://bioconductor.org/packages/release/bioc/html/clusterProfiler.html
seqLogo v1.5	Bembom, 2019	https://bioconductor.org/packages/release/bioc/html/seqLogo.html
Mclust v5.4.5	Scrucca et al., 2016	https://cran.r-project.org/web/packages/mclust/index.html
GREAT v4.0.4	McLean et al., 2010	RRID:SCR_005807; http://great.stanford.edu/public/html/
MEME suite	Machanick and Bailey, 2011	RRID:SCR_001783; http://meme-suite.org/
HOMER software suite v4.10	Heinz et al., 2010	RRID:SCR_010881; http://homer.ucsd.edu/homer/
BWA-MEM v0.7.13	Li, 2013	RRID:SCR_010910; https://sourceforge.net/projects/bio-bwa/files/
Picard Tools v2.0.1	http://picard.sourceforge.net/	RRID:SCR_006525
Samtools v1.8	Li et al., 2009	RRID:SCR_002105; http://www.htslib.org/
Deeptools v3.0.2-1	Ramírez et al., 2016	RRID:SCR_016366; https://deeptools.readthedocs.io/en/develop/
Integrated genome browser v9.0.2	Freese et al., 2016	RRID:SCR_011792; https://www.bioviz.org/
MACS2 v2.1.1.20160309	Zhang et al., 2008	RRID:SCR_013291; https://github.com/macs3-project/MACS
BEDtools v2.25.0	Quinlan and Hall, 2010	RRID:SCR_006646; https://bedtools.readthedocs.io/en/latest/#

RESOURCE AVAILABILITY

Lead contact
Further information and requests for resources and reagents should be directed to and will be fulfilled by the Lead Contact, N. Henriette Uhlenhaut: *henriette.uhlenhaut@tum.de*

Materials availability
Cell lines generated in this study can be requested without restriction upon completion of a material transfer agreement.

Data and code availability

The NGS datasets supporting the conclusions of this article are available at GEO (https://www.ncbi.nlm.nih.gov/geo/) with the following accession numbers:

RNA-Seq data: Expression in wild-type BMDMs, GSE137412, Expression in RAW264.7 cells (wild-type and *Setd1aDel/+*) and *Setd1b* knockout BMDMs, GSE137944. ChIP-Seq data: GR binding and H3K4me2/me3 in RAW264.7 cells, GSE138017, GR, SETD1A and CXXC1 binding, H3K4me1/me2/me3 and H3K27ac in BMDMs, GSE136070, GSM1446192 and GSM788651.

The mass spec proteomic datasets are available at the ProteomeXchange Consortium via the PRIDE repository with the dataset identifier PXD018077 (https://www.ebi.ac.uk/pride/archive/).

EXPERIMENTAL MODEL AND SUBJECT DETAILS

Animals

C57BL/6 mice were housed in a controlled environment (12h light/12h dark cycle, ~23°C). Mouse experiments were performed according to the rules and guidelines established by the Institutional Animal Committee at Helmholtz Center Munich. Ethical approval was obtained from the local animal welfare authority (LAGeSo Berlin; district government of Upper Bavaria).

GR floxed mice (Nr3c1 tm2Gsc, RRID:MGI:6257049) were crossed with hepatocyte-specific Albumin (Alb)-Cre mice obtained from JAX (B6.Cg-Tg(Alb-cre)21Mgn/J). Alb-Cre negative floxed littermates served as controls (Quagliarini et al., 2019). *R26^{creERT2/+}*, *Setd1a^{fl/fl}*, *R26^{creERT2/+}*, *Setd1b^{fl/fl}* and litter mate control (*R26^{creERT2/+}*) bones were kindly provided by Prof. Dr. K. Anastassiadis (TU Dresden, Germany) (Bledau et al., 2014). We exclusively study male mice. BMDMs were derived from 6-12 week old mice. Livers were harvested from 16 week old animals.

Cell lines

RAW264.7 cells (ATCC TIB-71, RRID:CVCL_0493; male, BALB/c-derivd) obtained from ATCC were maintained at sub confluent level in DMEM (10% FBS, including antibiotics) at 37°C and 5% CO2. Cells were regularly screened for mycoplasma.

METHOD DETAILS

Isolation and differentiation of BMDMs

Primary bone marrow-derived macrophages were isolated and differentiated in culture as previously described [10]. Shortly, bone marrow was harvested from 6-12 week old male mice with RPMI. Erythrocytes were lysed using AKC lysis buffer (1M NH4Cl, 1M KHCO3, 0.5M EDTA), and mononucleated cells were purified by Ficoll Paque gradient. Cells were differentiated in DMEM containing 20% FBS, 1% penicillin/streptomycin and 30% supernatant from L929 cells for 6 days on bacterial plates. Macrophages were harvested in Versene and seeded in macrophage serum-free medium.

Cells were treated with vehicle (0.1% EtOH and PBS), 1μM dexamethasone (in EtOH) for 16h or 0.1% ethanol and/or lipopolysaccharide (LPS, 100ng/ml, Sigma-Aldrich) for 3h (ChIP-Seq) or 6h (RNA-Seq, qPCR) unless indicated otherwise.

For deletion of *Setd1a* and *Setd1b* in bone marrow-derived macrophages of *R26^{creERT2/+}*, *Setd1a^{fl/fl}* or *R26^{creERT2/+}*, *Setd1b^{fl/fl}* mice, cells were treated with 1μM 4-hydroxytamoxifen (Sigma-Aldrich) after 3 days in differentiation medium.

Cell culture

RAW264.7 cells were treated with vehicle (0.1% EtOH and PBS), LPS (100ng/ul in D-PBS, Sigma-Aldrich) or dexamethasone (1μM in EtOH, Sigma-Aldrich) and LPS for the indicated time periods. Unless stated otherwise, treatment times were 16h Dex and 3h LPS for ChIP or 6h LPS for RNA, respectively. 3h IFN-β1 treatment (10ng/ml, R&D Systems) was performed alone or in combination with 100ng/ml LPS. 3h incubation with 0.05% BSA/PBS was used as vehicle control. Spike-in chromatin was generated from *Drosophila* S2 cells (a gift from P. Becker, RRID:CVCL_IZ06) grown in T175 flasks with Schneider's *Drosophila* medium supplemented with 10% FBS and 1% Penicillin/Streptomycin at 28°C under normal atmosphere.

Generation of CRISPR mutant cell lines

GuideRNAs were designed using the e-crisp tool (Heigwer et al., 2014) and cloned into pU6.chimeric via BbsI overhangs (a gift from I. Burtscher, Helmholtz Zentrum Muenchen). For mutation of RAW264.7 cells, pU6.chimeric.gRNA (Table S6), pCAG.Cas9D10A-EGFP (expressing Cas9 nickase, a gift from I. Burtscher) and a single strand DNA repair template (IDT, see Table S6)) were electroporated using the NEON electroporation system, FACS sorted after 24h and seeded as single clones. Positive clones were identified by genotyping PCR (Table S6 for oligo sequences) and PCR products were sequenced. *Setd1a^{DelSet/+}* was generated by introduction of a premature STOP codon after exon 14, leading to a destabilized form of SETD1A (see Figure S5A).

Nuclear extraction and Co-ImmunoPrecipitation

Nuclear extraction was performed using standard protocols. Shortly, cells were harvested by washing in ice-cold PBS and collected by centrifugation (300 g at 4°C). Cell lysis was performed in hygroscopic conditions using V1 buffer (10mM HEPES-KOH pH 7.9; 1.5mM MgCl2; 10mM KCl and 1μM dexamethasone, 0.5mM DTT, 0.15% NP40, protease inhibitors and PhosphoSTOP) while

douncing on ice. Crude nuclei were collected by centrifugation (2,700 g at 4°C) and nuclear lysis was performed in V2 buffer (420mM NaCl; 20mM HEPES-KOH pH 7.9; 20% glycerol; 2mM MgCl2; 0.2mM EDTA and 1μM dexamethasone; 0.5mM DTT; 0.1% NP40; protease inhibitors and PhosphoSTOP) while incubating for 1h at 4°C and subsequent centrifugation at 21,000 g (4°C). Supernatants were directly processed for co-IP. Co-IP was performed by diluting 200 μg 1:1 in AM100 (100mM KCl, 5mM MgCl2, 20mM Tris (pH 8.0), 0.2mM EDTA and 20% glycerol) with EDTA-free proteinase inhibitors and pre-cleared with pre-blocked sheep α-rabbit or sheep α-mouse IgG Dynabeads for 2h at 4°C while agitating. IPs were incubated with 1μg of antibody (Key resources table) for 2h at 4°C. Subsequently, pre-blocked sheep α-rabbit or sheep α-mouse IgG Dynabeads (ThermoFisher Scientific) were collected after 3 washes with buffer AM100 plus 0.5% Triton. Bound proteins were eluted in Laemmli buffer and analyzed by western blots. For Co-IP from whole cell lysates, RAW264.7 cells were lysed in NP40 buffer (25mM Tris pH 7.5, 150mM NaCl, 1mM EDTA, 1% NP40, 5% glycerol, freshly added phosphatase and proteinase inhibitors), sonicated for 15 s and cleared by spinning 10min at 12,000xg. After preclearing samples were diluted 1:5 in Tris IP buffer (20mM Tris pH 7.5, 2mM MgCl₂, 100mM NaCl, 0.2mM EDTA, 0.1% Triton X-100, freshly added phosphatase and proteinase inhibitors) for incubation with 1ug of primary antibody (Key resources table) overnight at 4°C. Pre-blocked beads were added for 3h on the next day and proteins eluted from the beads after three washes with Tris-IP buffer, one wash with Tris-IP buffer including 500nM NaCl and 1 wash of Tris-IP buffer including 500nM NaCl and 1% Triton X-100.

Western Blotting
Standard procedures were applied for western blotting using precast Bis-Tris SDS-PAGE 4%–12% gradient gels. Histones were run on 12% Bis-Tris gels. Antibodies are listed in the Key resources table. Specificity of H3K4me1/me2/me3 antibodies was tested in peptide competition western blots (data not shown).

RNA isolation and qRT-PCR
Total RNA from 200,000 (qPCR) or 1 million cells (RNA-Seq) was isolated using the RNeasy Mini kit (QIAGEN) with on-column DNaseI digest, following the manual. RNA was measured with Nanodrop2000. 500ng RNA were reverse transcribed using a Reverse Transcription Kit (QIAGEN) according to manufacturer's instructions. Quantitative PCR was run on Quantstudio 6/7 using SYBR Green in standard curve mode. Primer pairs are listed in Table S6. Gene expression was normalized to the housekeeping gene *Rplp0*. Values from independent experiments were standardized using z-scores. Plots show means with standard deviations as error bars. Individual data points are given as dots.

RNA-Seq
RNA quality was verified using an Agilent2100 Bioanalyzer with RNA 6000Nano Reagents. Library preparation and rRNA depletion was performed using the TruSeq Stranded mRNA Library Prep Kit starting with 500ng total RNA as input for each sample. Libraries were sequenced on the Illumina HiSeq4000. Experiments were performed in triplicates.

ChIP-Seq
For ChIP experiments, 20 million cells (BMDMs, RAW264.7 or S2 cells) were treated as indicated above. Mouse livers were harvested at night (peak of corticosterone levels) and snap frozen in liquid nitrogen. 250mg of liver tissue were thawed on ice and incubated with 1% formaldehyde for 15min while homogenizing (Dounce) at room temperature. Cells were washed in D-PBS and fixed either in 1% formaldehyde (methanol-free) for 10min or in 2mM disuccinimidyl-glutarate for 30min plus 10min 1% FA (see Table S5). Formaldehyde was quenched with 150mM glycine, and cells were washed with D-PBS, pelleted and stored at −80°C or directly processed for ChIP using 2μg (transcription factor/coregulator) or 1μg (histones) of antibody (Key resources table) as previously described (Nelson et al., 2006; Quagliarini et al., 2019).

For ChIP-Seq, 40 million cells per sample were used for GR and COMPASS proteins. For histone marks, 20 million cells per sample were used. ChIP-Seq was performed with the following modifications: Chromatin was sonicated using a Bioruptor pico (Diagenode) with either 8μg (GR, COMPASS) or 3μg antibody (histones): see Key resources table. Purified DNA was quantified using Qubit. Library preparation was performed from 5ng of ChIP DNA using the Kappa Hyperprep and library amplification kits according to the manufacturer's manual (Roche). Libraries were sequenced on an Illumina HiSeq4000. A minimum of two replicates per condition was performed (See Table S5).

NGS Data analysis
RNA-Sequencing
NGS data quality was assessed with FastQC (RRID:SCR_014583, http://www.bioinformatics.babraham.ac.uk/projects/fastqc/). Gene-level quantification was performed with Salmon version 0.10.2 (RRID:SCR_017036 (Patro et al., 2017)). Settings were: -libType A, -gcBias, -biasSpeedSamp 5 using the mm10 (GRCm38.p6) reference transcriptome provided by Ensembl (RRID:SCR_002344 (Cunningham et al., 2019)). Gene count normalization and differential expression analysis was performed with DESeq2 version 1.22.0 (RRID:SCR_015687 (Love et al., 2014)) after import of gene-level estimates with "tximport" (RRID:SCR_016752 (Soneson et al., 2015)) in R (RRID:SCR_001905, R version 3.6.1 (R Core Team, 2017)).

For gene annotation, Ensembl gene Ids were mapped to MGI symbols using the Bioconductor package "biomaRt" version 2.38 (RRID:SCR_002987 (Durinck et al., 2009)) and genome information was provided by Ensembl (GRCm38.p6 (Cunningham et al., 2019)). Genes with a minimal mean count across samples (baseMean) of 50, fold change of 1.5 and Benjamini-Hochberg-adjusted p value < 0.05 were called significantly changed. Significance of the genotype contribution to the treatment effect (Dex versus veh; LPS+Dex versus LPS) was determined by log-likelihood-ratio test comparing the full model ~genotype+treatment+treatment:genotype with the reduced model ~treatment. p values are Benjamini-Hochberg adjusted. The dependency of the Dex response from genotype and treatment time was accessed by likelihood-ratio test between the full model (~genotype + treatment + treatment:genotype) and the reduced model (~genotype + treatment).

Gene Ontology biological process enrichment was performed using GOrilla (RRID:SCR_006848 (Eden et al., 2009)) using the un-ranked list mode. All genes expressed with a mean expression level over 50 counts were used as the background set for macro-phages or RAW264.7 cells respectively. GO terms were significantly enriched with a FDR < 0.01 and a set size smaller than 500 genes per term. Redundant terms were removed manually.

ChIP-Sequencing

ChIP-Seq reads were aligned to the reference genome mm10 (Ensembl GRCm38.p6 (Cunningham et al., 2019)) using BWA-MEM version 0.7.13 (RRID:SCR_010910 (Li, 2013)) and PCR duplicates were removed using Picard Tools version 2.0.1 (RRID:SCR_006525, http://picard.sourceforge.net/). Samples with duplication levels above 80% were excluded from further anal-ysis. For visualization, bam files were filtered for properly paired and mapped reads with Samtools version 1.8 (RRID:SCR_002105 (Li et al., 2009)) and converted to bigwig files merging 10 bp per bin using "bamCoverage" from the Deeptools package version 3.0.2-1 (RRID:SCR_016366 (Ramírez et al., 2016)). Tracks were visualized using the integrated genome browser (IGB, RRID:SCR_011792 (Freese et al., 2016)) version 9.0.2.

Peaks were called using MACS2 version 2.1.1.20160309 (RRID:SCR_013291) with an FDR threshold of 0.1 for reproducible peaks and FDR = 0.05 for the generation of a "peak union" (Zhang et al., 2008). Blacklisted regions (http://mitra.stanford.edu/kundaje/akundaje/release/blacklists/mm10-mouse/mm10.blacklist.bed.gz) were removed from the called peaks. Peaks were termed repro-ducible when they were called in two independent ChIP-Seq experiments and overlapped for 50% of the mean peak width. We also identified a "peak union" merging any peak called by MACS2 in any of the experiments.

For Venn diagrams, peaks overlapping each other with a minimum of 1bp on either strand were termed overlapping. The overlap was determined using the "GenomicRanges" package version 1.36.1 (RRID:SCR_000025 (Lawrence et al., 2013)).

Heatmaps were generated using HOMER software suite version 4.10 (RRID:SCR_010881 (Heinz et al., 2010)) and visualized with the "ggplot2" package version 3.2.1 (RRID:SCR_014601 (Wickham, 2016)) or the "gplots" package (https://github.com/talgalili/gplots/) version 3.0.1.1 in R 3.6.1 (RRID:SCR_014601 (R Core Team, 2017)). Heatmaps represent the mean the mean and the stan-dard deviation of at least two replicates (Table S5).

Bigwig files were scaled according to DESeq2 scale factors estimated from reads covering the whole peak union ("static peak" normalization), assuming that most of the peaks do not change their coverage in response to dexamethasone. When spike-in ChIP-Seq was performed, the data were normalized by the spike-in ratios in cases where the DESeq2 assumption (Love et al., 2014) might be violated (e.g., Setd1a^Del/+ mutants). All scaling factors are provided in Table S5.

Peaks were annotated to the nearest TSS using the "ChIPpeakAnno" package version 3.18.2 (RRID:SCR_012828 (Zhu et al., 2010)) and called intergenic when more than 1kb away from any gene.

Read counts covering peaks were obtained using BEDtools version 2.25.0 (RRID:SCR_006646 (Quinlan and Hall, 2010)) (Table S5).

Immunoprecipitation (IP) efficiencies were defined as portion of mapped unique read pairs covering the peak union. Samples with an IP efficiency below 15% were excluded from further analysis.

For Volcano plots, correlations, and modeling, reads were counted after adjustment to a unique peak length of 588bp (4 nucleo-somes) around the peak center and scaled afterward, as described above.

Differential ChIP-Seq analysis was performed with "DESeq2" (RRID:SCR_015687 (Love et al., 2014)) using the above calculated scaling factors. Log2FoldChanges always refer to the comparison between Dex plus LPS and LPS only treatments, unless stated otherwise.

For spike-in normalization of H3K4me1/me2/me3 ChIP-Seq in Setd1a^Del/+ mutants, reads were mapped to the murine reference genome mm10 and the Drosophila melanogaster genome build dm6 (Ensembl BDGP6 release 78 (Cunningham et al., 2019)). Scaling factors for bigwig files were determined as the fly-specific reads-in-peaks ratio between all samples, and adjusted for differences in IP efficiencies between samples for the spiked fly S2 cell chromatin as follows (see Table S5). Variations in the Drosophila ChIP were assumed to account for technical variations between samples and therefore applied to the mm10-mapped reads (Egan et al., 2016). Scaling factors for heatmaps and genome-browser tracks were calculated as above.

Statistical analysis and visualization was performed in R 3.6.1 (RRID:SCR_001905 (R Core Team, 2017)).

For KEGG pathway enrichment, the "clusterprofiler" package was used (RRID:SCR_016884 (Yu et al., 2012)). Results are dis-played as circles reflecting the gene ratio (number of genes in a given subset covered by the pathway, divided by the number of genes in that pathway) and shades representing the Benjamini-Hochberg adjusted hypergeometrical p value.

For enrichment of Gene Ontology biological processes, peak positions were assigned to the nearest gene, and enrichment analysis was performed with GREAT (RRID:SCR_005807 (McLean et al., 2010)). Bonferroni-adjusted hypergeometrical p values are shown, and terms were significantly enriched and reported when the p value was < 0.01.

Motif enrichment was performed on peaks trimmed to 100bp around the peak center with MEME suite (RRID:SCR_001783 (Machanick and Bailey, 2011)) in enrichment or differential mode as indicated in the figure legends. MEME parameters were set to: "-dna -meme-mod anr -meme-minw 6 -meme-maxw 30 -meme-nmotifs 10 -meme-p 10" using the JASPAR (2018 version, RRID:SCR_003030 (Khan et al., 2018)), Uniprobe (RRID:SCR_005803 (Newburger and Bulyk, 2009)) and SwissRegulon (RRID:SCR_005333 (Pachkov et al., 2013)) databases. Motifs were visualized from position-weight matrices obtained from the HO-COMOCO (version 11 (Kulakovskiy et al., 2018)) or JASPAR databases with the "seqLogo" package version 1.5 in R 3.6.1 (Bembom, 2019). Centrimo motif enrichment was performed to identify centrally enriched motifs, and MEME was used for motif enrichment within a given peak set.

Model-based clustering was performed with the "mclust" package version 5.4.5 in R 3.6.1 (Scrucca et al., 2016). Features were quantified at GBSs extended by 588 bp and scaled to unit length. Bayesian Information Criterion (BIC) was used to determine cluster numbers and the best fitting model. The model selected in this paper is VEE (diagonal distribution with variable volume and ellipsoidal shape).

ChIP-qPCR

For ChIP-qPCR, 20 million cells were used per sample. A minimum of two independent experiments with two biological replicates each were performed.

Cells were fixed and processed as described above with 1μg of antibody against histone marks and 3μg of antibody against other proteins (Key resources table).

qPCRs were run on Quantstudio 6/7 in standard curve mode using SYBR Green and the primers listed in Table S6. Enrichment was calculated as percent of input and ChIPs against histone marks were normalized to total histone H3. To account for inter-experimental variation, ChIP results from independent experiments were standardized using z-scores. Plots show means with standard deviations as error bars. Individual data points are given as dots.

Spike-in ChIP

Spike-in ChIP-Seq/qPCR was performed as indicated above with addition of 5% (ChIP-Seq) or 10% (ChIP-qPCR) *Drosophila* S2 chromatin to all samples before sonication. qPCRs against genomic regions positive for *Drosophila* H3K4me1/me2/me3, H3K27ac and H3 were used for normalization (see Table S5). Ct-values were corrected for PCR efficiency; enrichment over input was calculated and normalized to the *Drosophila* signal (Egan et al., 2016). Histone modifications were additionally normalized to total H3 (see above).

ChIP-MS interactomes

For mass spectrometric analysis of purified co-enriched proteins, GR ChIP was performed as described above, followed by proteomics. Chromatin was sonicated to an average size of 200 bp using the Bioruptor pico (Diagenode). After incubation with primary α-GR antibody (#sc-1004X SantaCruz, RRID:AB_2155786) or rabbit IgG (#2729, Cell Signaling Technology, RRID:AB_1031062), samples were processed as described in (Hemmer et al., 2019; Quagliarini et al., 2019).

In detail, cells were treated and crosslinked as for ChIP-Seq, lysed in IP-buffer (50 mM Tris-HCl, pH 8.0, 100 mM NaCl, 5 mM EDTA, 0.3% SDS, 1.7% Triton X-100) and chromatin sonicated to an average size of 200bp. After overnight immunoprecipitation with α-GR antibody antibody, or rabbit IgG, antibody-bait complexes were captured by ChIP-Grade Protein G Agarose Beads (#9007 Cell Signaling Technology), washed three times with wash buffer A (50mM HEPES pH 7.5, 140mM NaCl, 1% Triton), once with wash buffer B (50mM HEPES pH 7.5, 500mM NaCl, 1% Triton), and twice with TBS. Beads were incubated for 30min with elution buffer 1 (2M Urea, 50mM Tris-HCl pH 7.5, 2mM DTT, 20μg/ml trypsin) followed by a second elution with elution buffer 2 (2M Urea, 5 mM Tris-HCl pH 7.5, 10mM Chloroacetamide) for 5min. Both eluates were combined and further incubated at room temperature overnight. Tryptic peptide mixtures were acidified to 1% TFA and desalted with Stage Tips containing three layers of C18 reverse phase material and analyzed by mass spectrometry.

Peptides were separated on 50cm columns packed with ReproSil-Pur C18-AQ 1.9 μm resin (Dr. Maisch GmbH). Liquid chromatography was performed on an EASY-nLC 1200 ultra-high-pressure system coupled through a nanoelectrospray source to a Q-Exactive HF mass spectrometer (Thermo Fisher Scientific). Peptides were loaded in buffer A (0.1% formic acid) and separated applying a non-linear gradient of 5%–60% buffer B (0.1% formic acid, 80% acetonitrile) at a flow rate of 250nl/min over 120min. Data acquisition switched between a full scan (60K resolution, 20ms max. injection time, AGC target 3e6) and 10 data-dependent MS/MS scans (15K resolution, 60ms max. injection time, AGC target 1e5). Isolation window was set to 1.4 and normalized collision energy to 27. Multiple sequencing of peptides was minimized by excluding the selected peptide candidates for 30 s.

Data analysis

Raw mass spectrometry data were analyzed with MaxQuant (v1.5.1.1, RRID:SCR_014485) (Cox and Mann, 2008). Peak lists were searched against the mouse UniprotFASTA database (2015_08 release) combined with 262 common contaminants by the integrated Andromeda search engine. False discovery rate was set to 1% for both peptides (minimum length of 7 amino acids) and proteins. 'Match between runs' (MBR) with a maximum time difference of 0.7min was enabled. Relative protein amounts were determined by the MaxLFQ algorithm with a minimum ratio count of two.

Statistical analysis of LFQ derived protein expression data was performed using Perseus (v.1.5.1.1, RRID:SCR_015753) (Tyanova and Cox, 2018). Protein entries referring to contaminants, proteins identified via matches to the reverse database, and proteins

identified only via modified sites, were removed, LFQ values log2 transformed and missing values imputed from a normal distribution applying a width of 0.2 and a downshift of 1.8 standard deviations. Significant outliers were defined by permutation-controlled Student's t test (FDR < 0.01, s0 = 1) comparing triplicate ChIP-MS samples for each antibody, requiring at least two valid values in the GR replicates.

Functional annotation of proteins significantly (p < 0.05) enriched over IgG, was performed with GOrilla (RRID:SCR_006848 (Eden et al., 2009)) in the "two unranked lists" mode, and all detected proteins used as the background set, using the Gene Ontology (GO) 'Biological Processes'. The most specialized GO terms with significant enrichment (FDR < 0.05) are reported.

QUANTIFICATION AND STATISTICAL ANALYSIS

For all experiments, normal distribution of the data was assessed by Shapiro-Wilk test, and plotting the data distribution as histograms if the Shapiro-Wilk test was slightly significant (0.001 < p < 0.05). Log2 transformation of the data was performed to obtain normal distribution as indicated. Equal variance of sample groups was tested by Bartlett test (parametric) or Levene test (non-parametric). Significance was assessed by Student's t test in case of normal distributed homoscedastic data, Welch test in case of normal distributed heteroscedastic data and Wilcoxon-Mann-Whitney test in all other experiments with single factor designs. In multi-factor design experiments, significance was tested by analysis of variance (ANOVA) with post hoc pairwise t test (homoscedastic, normal distributed data) or Kruskal-Wallis test with post hoc Wilcoxon-Mann-Whitney (homoscedastic, non-normal data) or Dunn's test (heteroscedastic, non-normal data), respectively. P values were Benjamini-Hochberg adjusted. Unless stated otherwise, p values are only indicated if significant (p < 0.05).

Bar plots display the mean and individual data points are indicated. The standard deviation is given as error bars unless indicated otherwise. Detailed information for each experiment can be found in the figure legends.